Casein Kinase II Phosphorylation of Spt6 Enforces Transcriptional Fidelity by Maintaining Spn1-Spt6 Interaction

Raghuvar Dronamraju[1,2], Jenny L. Kerschner[1,2,5,^], Sarah A. Peck[3,5], Austin J Hepperla[4,5], Alexander T. Adams[1], Katlyn D. Hughes[3], Sadia Aslam[1#], Andrew R. Yoblinkski[1], Ian J. Davis[4], Amber L. Mosley[3], and Brian D. Strahl[1,2,6]

[1]Department of Biochemistry & Biophysics, University of North Carolina School of Medicine, Chapel Hill, NC 27599, USA
[2]Lineberger Comprehensive Cancer Center, University of North Carolina School of Medicine, Chapel Hill, NC 27599, USA
[3]Indiana University School of Medicine, Department of Biochemistry and Molecular Biology, Indianapolis, IN 46202, USA
[4]Curriculum in Genetics and Molecular Biology, University of North Carolina at Chapel Hill, Chapel Hill, NC 27599, USA

[5]These authors contributed equally

[6] Lead Contact

^Current Address: Department of Genetics and Genome Sciences, Case Western Reserve University, Cleveland, OH 44016, USA
[#]Current Address: American University of the Caribbean School of Medicine, Jordan Dr., Saint Marteen

Keywords: histone chaperone, casein kinase II, Spt6, histone gene transcription and transcriptional fidelity.

Running Title: CKII-dependent Spt6 phosphorylation and antisense transcription.

Highlights

- Casein Kinase II (CKII) phosphorylates the unstructured N-terminus of Spt6.
- CKII phosphorylation of Spt6 is required to prevent sense and antisense transcription.
- In Spt6 mutants, antisense transcripts arise predominantly from the 5'-ends of genes where nucleosomes become depleted.
- CKII phosphorylation of Spt6 promotes Spt6-Spn1 interaction to reinforce nucleosome occupancy and prevent cryptic transcription

SUMMARY

Spt6 is a histone chaperone that associates with RNA polymerase II and deposits nucleosomes in the wake of transcription. Although Spt6 has an essential function in nucleosome deposition, it is not known whether this function is influenced by post-translational modification. Here, we report that casein kinase II (CKII) phosphorylation of Spt6 is required for nucleosome occupancy at the 5'-ends of genes to prevent aberrant antisense transcription and enforce transcriptional directionality. Mechanistically, we show that CKII phosphorylation of Spt6 promotes interaction of Spt6 with Spn1 – a binding partner required for chromatin reassembly and full recruitment of Spt6 to genes. Our study defines a previously unknown function for CKII phosphorylation in transcription and highlights the importance of post-translational modification in histone chaperone function.

INTRODUCTION

DNA associates with histone proteins (H2A, H2B, H3, and H4) to form nucleosomes – the fundamental repeating unit of chromatin. To access the underlying DNA, processes such as DNA replication, transcription, and repair depend on histone chaperones and ATP-dependent chromatin remodelers to dismantle and reassemble chromatin structure (Eitoku et al., 2008; Erdel and Rippe, 2011; Ho and Crabtree, 2010; Lai and Wade, 2011; Wilson and Roberts, 2011). In budding yeast, there are two well-characterized transcription-associated histone chaperones: Facilitates Chromatin Transcription (FACT), composed of Spt16 and Pob3 (in conjunction with NHP6A/B), and Spt6, which function during transcription elongation (Bortvin and Winston, 1996; Endoh et al., 2004; Formosa, 2003; Hartzog et al., 1998; Jeronimo and Robert, 2016; Kaplan et al., 2005; McCullough et al., 2015; Svejstrup, 2003).

Recent findings show that Spt6 directly binds to a phosphorylated linker domain in RNA Polymerase II (RNAPII) via its tandem Src2 homology domain (tSH2) (Sdano et al., 2017); furthermore studies from several labs find that Spt6 has capacity to also bind to the serine 2 and/or tyrosine 1 phosphorylated C-terminal domain (CTD) of RNAPII (Close et al., 2011; Dengl et al., 2009; Diebold et al., 2010b; Liu et al., 2011; Sun et al., 2010; Yoh et al., 2007). In addition, Spt6 regulates chromatin structure through the ability of its highly acidic (pI ~4.2) and unstructured N-terminus to bind histones/nucleosomes (Bortvin and Winston, 1996; McCullough et al., 2015). This same acidic and unstructured region also contains a binding site for Spn1 [Interacts with SUPT6H (IWS1) in metazoans], a binding partner of Spt6 that competes with Spt6 to bind to nucleosomes and prevent premature recruitment of the Swi/Snf complex during transcription elongation (McDonald et al., 2010; Zhang et al., 2008).

With its ability to bind phosphorylated RNAPII, Spt6 plays an important role in nucleosome deposition and the control of downstream processes such as termination, and mRNA export/stability (Andrulis et al., 2002; Dronamraju et al., 2018; Mayer et al., 2012; Winston, 2001).

Along with Spt6, the RNAPII elongation machinery is composed of many other factors, including, but not limited to, Spt4/5 (DSIF), the Polymerase Associated Factor Complex (PAF-C), Spt2, Dst1/TFIIS, and the Ctk1 and Bur1 kinases that modify the CTD of RNAPII and (for Bur1) Spt5 (Cui et al., 2016; Dronamraju and Strahl, 2014; Kwak and Lis, 2013; Youdell et al., 2008). In addition to all the above-mentioned factors, casein kinase II (CKII) also co-purifies with Spt16, Spt6, and the RNAPII holoenzyme (Bedard et al., 2016; Krogan et al., 2002; Kurat et al., 2011). Although studies have revealed a requirement for CKII during transcription initiation and elongation in mammalian and yeast cells (Basnet et al., 2014; Chapman et al., 2004), it is not known exactly how CKII functions in these processes.

We have reported that CKII phosphorylates members of the PAF-C *in vivo* and *in vitro*, and this phosphorylation is essential for maintenance of the global level of histone H2BK123 mono-ubiquitination (H2BK123ub1) (Bedard et al., 2016). Additionally, other factors associated with transcription elongation (*e.g.*, Spt6, Spt16, PAF-C, RNAPII holoenzyme) possess consensus CKII phosphorylation sites (Bhat et al., 2013; Krogan et al., 2002), but it has not been determined whether these proteins are modified by CKII and whether modification has a function in transcription elongation. In this report, we show that CKII phosphorylates multiple residues within the N-terminus of Spt6 – a region of Spt6 that interacts with H3/H4 and Spn1 (Bortvin and Winston, 1996; McDonald et al., 2010). Mutation of these CKII sites in Spt6 to prevent phosphorylation (S→A, hereafter $spt6_{S8\rightarrow A8}$) resulted in reduced global nucleosome occupancy and aberrant antisense transcription from the 5'-ends of genes. A version of Spt6 that mimics constitutive Spt6 phosphorylation (S→E, hereafter $spt6_{S8\rightarrow E8}$) largely rescued these phenotypes. These findings agree with a recent report that also characterized Spt6 phosphorylation by CKII (Gouot et al., 2018). Mechanistically, we found that CKII phosphorylation of Spt6 is required for the full association of Spt6 with Spn1, which is required for nucleosome reassembly and for the recruitment of chromatin remodelers that aid in transcription elongation (Zhang et al., 2008). Our

results suggest that, during transcription elongation, CKII phosphorylation of Spt6 facilitates a phospho-dependent interaction between Spt6 and Spn1 that functions to promote nucleosome occupancy at the 5'-ends of genes to enforce the accuracy and directionality of transcription.

RESULTS

The N-terminus of Spt6 is Phosphorylated by CKII

Recently, we characterized a protein interaction network involving CKII, FACT, PAF-C, and other members of the RNAPII transcription elongation complex (Bedard et al., 2016). Our study revealed that CKII phosphorylates PAF-C members and regulates PAF-C-dependent H2BK123ub1. We also discerned potential CKII phosphorylation sites in other co-associated transcription elongation factors (*e.g.*, Spt16, Pob3, Spt2, and Spt6) suggesting that CKII might also regulate the function of these transcription elongation factors. Thus, we employed a temperature sensitive CKII strain (*cka1Δ cka2-8*; hereafter *ck2-ts*) to determine whether other transcription-associated histone modifications would be affected under conditions in which CKII activity was compromised (Hanna et al., 1995). As previously demonstrated, at the temperatures of 25°C and 37°C (Bedard et al., 2016; Hockman and Schultz, 1996), the level of H2BK123ub1 in the *ck2-ts* strain was partially reduced, whereas there was no effect on the levels of H3 lysine 4 (H3K4) methylation or H3 lysine 79 (H3K79) methylation (Figure S1A). Unexpectedly, we also found that the absence of CKII activity caused a dramatic reduction in global H3K36me3 levels (Figure S1A), suggesting that CKII activity regulates some aspect of the Spt6-Set2-H3K36me axis (Dronamraju and Strahl, 2014).

Because CKII and Spt6 co-purify together as had been reported (Krogan et al., 2002), we hypothesized that CKII activity might be important for H3K36 methylation through phosphorylation of Spt6. In agreement with Krogan et al., we confirmed the association of CKII with Spt6 in co-immunoprecipitation studies wherein both CKII subunits, *CKA1* and *CKA2*, were tagged with a 6HA epitope (Janke et al., 2004) in a FLAG-Spt6 strain (Figure S1B). Given this association, we

inspected the Spt6 coding sequence to determine whether it contains sequence motifs that satisfy the CKII phosphorylation consensus [(S/T)XX(D/E)] (Hanna et al., 1995). Our analysis revealed that the acidic N-terminus of Spt6 (aa 1-300) contains eight consensus CKII sites (Table S1 and see schematic in Figure 1A). To comprehensively verify these probable sites of Spt6 phosphorylation, we performed affinity purification of TAP- and FLAG-tagged Spt6 and subjected the purified proteins to mass spectrometry analysis and phospho-peptide mapping. As shown in Figure 1A, we identified many phosphorylation sites that occur at CKII consensus sites, primarily within the N-terminus of Spt6. Spt6 is not 100% phosphorylated by CKII when purified, indicating that these sites exists in both modified and unmodified forms. A comprehensive summary of these sites is presented in Figure 1A and Table S1.

We next asked whether the CKII phosphorylation sites detected in Spt6 would be sensitive to the absence of CKII. We performed quantitative proteomics and analyzed affinity purified FLAG-Spt6 from WT and *ck2-ts* cells after shifting the cells to restrictive temperature to attenuate CKII activity (Figure 1B). In brief, equal numbers of yeast cells were grown in media containing either light (*ck2-ts*) or heavy (WT) arginine and lysine to perform stable isotopic labeling (a.k.a., SILAC Arg10 Lys8; (de Godoy, 2014)). We performed quantitation using area under the curve measurements for MS1 peak area for the heavy and light peptides. When CKII was inactivated, abundance changes were observed in both unmodified and phosphorylated peptides containing serine residues 94, 134, and 136; which are CKII consensus sites (Figure 1C). Phosphorylated Spt6 peptides, shown in red, encompassing S134 and S136 showed a 1.3-fold decrease in the *ck2-ts* mutant, whereas un-phosphorylated forms, shown in yellow, of the same peptides were enriched by ~4-fold in the *ck2-ts* mutant. Although we did not observe large change in unmodified S94-containing peptides, we did observe decreases in S94 phosphopeptides ranging from 1.5- to just over 2-fold (Figure 1C). Representative spectra of Spt6 phospho-sites are shown in Supplementary Figures S2A-S2H. These results provide strong evidence that Spt6 is a target of CKII phosphorylation *in vivo*.

To provide further evidence that CKII directly targets Spt6, we performed *in vitro* kinase assays as described previously (Bedard et al., 2016) using purified CKII enzyme with i) a bacterially expressed N-terminal fragment of Spt6 containing all of the CKII consensus sites (Spt6 1-300), and ii) full-length FLAG-Spt6 purified from asynchronously growing yeast cells (FL Spt6). As controls for these experiments, we generated mutant versions of recombinant and full-length Spt6 proteins in which all eight consensus CKII sites were changed to alanine to prevent phosphorylation ($Spt6_{S8\rightarrow A8}$ 1-300 and FL $Spt6_{S8\rightarrow A8}$, respectively). As shown in Figure 1D, following incubation with 500 Units of CKII enzyme for 30 minutes at 30°C, we observed robust phosphorylation of the WT Spt6 fragment (1-300 aa), whereas the $Spt6_{S8\rightarrow A8}$ 1-300 mutant protein showed only background signal. The full-length WT and mutant versions of FLAG-Spt6 purified from yeast cells also exhibited similar behavior (Figure 1E). These results establish that CKII is a *bona fide* kinase for Spt6, and further, that all eight CKII consensus sites identified account for the majority, if not all, of the CKII activity that occurs on Spt6.

Because CKII phosphorylates Spt6 *in vivo* and *in vitro*, we next asked whether phosphorylation would have a direct consequence on Spt6 protein stability. To this end, we performed cycloheximide chase experiments in WT and our *spt6* mutant strain in which we changed all eight CKII sites to alanine ($spt6_{S8\rightarrow A8}$). Intriguingly, we found that Spt6 was degraded in WT cells within 2 h, whereas the degradation kinetics were faster in the $spt6_{S8\rightarrow A8}$ mutant and occurred within 1 h of cycloheximide treatment (Figure 1F). The kinetics of Spt6 degradation were similar to the WT in the $spt6_{S8\rightarrow E8}$ mutant in which all eight CKII sites were changed to glutamic acid to mimic phosphorylation (Figure S2I). These results suggest that CKII phosphorylation of Spt6 is important for its protein stability, which we surmise is because CKII phosphorylation of Spt6 is important to its function.

To further understand the biological significance of these mutations under different physiological conditions, we subjected the WT, $spt6_{S8\rightarrow A8}$ and $spt6_{S8\rightarrow E8}$ strains to different growth

conditions. As a control for these studies, we included several previously characterized *spt6* mutant alleles, $spt6_{tSH2\Delta}$ and *spt6-F249K* (Close et al., 2011; McDonald et al., 2010) and the *ck2-ts* strain (Hanna et al., 1995). The $spt6_{tSH2\Delta}$ mutant contains a deletion of the Spt6 tandem SH2 domain (tSH2) that is responsible for interaction with RNAPII, whereas the *spt6-F249K* mutant partially impairs the association of Spt6 with Spn1. As expected from previous analyses, the $spt6_{tSH2\Delta}$, *spt6-F249K,* and *ck2-ts* strains showed a slow growth phenotype at 30ºC (Figure 1G) (Bedard et al., 2016; Diebold et al., 2010b; McDonald et al., 2010). The *spt6-F249K* mutation was sick at elevated temperature (37ºC) and on plates containing the replication inhibitor hydroxyurea (HU) (Figure 1G) (Diebold et al., 2010a; Dronamraju and Strahl, 2014; McDonald et al., 2010). These phenotypes were similar to the *ck2-ts* strain (Figure 1G). In contrast, deletion of the tSH2 domain of Spt6 caused HU sensitivity but did not affect growth at 37ºC (Figure 1G) (Diebold et al., 2010b).

Based on the foregoing phenotypes, we tested our $spt6_{S8\rightarrow A8}$ and $spt6_{S8\rightarrow E8}$ mutants at 37ºC and in the presence of HU. Both mutant strains demonstrated growth patterns similar to WT at 30ºC in YPD (Figure 1H). At both 37ºC and on plates containing HU, the $spt6_{S8\rightarrow A8}$ mutant showed a severe growth defect similar to the *spt6-F249K* and *ck2-ts* strains (Figure 1G). Conversely, the $spt6_{S8\rightarrow E8}$ phospho-mimic mutant grew almost like WT at 37ºC or in the presence of HU (Figure 1H). These results further suggest that Spt6 phosphorylation by CKII is important for its function. Furthermore, the HU phenotypes suggest that Spt6 may have a role in DNA replication or is important for the transcription of genes required for replication or cell cycle control.

Finally, to ascertain whether the biological phenotypes observed in the $spt6_{S8\rightarrow A8}$ strain were dependent on all eight CKII sites, or just a subset, we created two additional serine to alanine cluster mutants of Spt6 to examine the effect of mutating either 3 or 5 of the CKII sites in Spt6 in combination: s$pt6_{S3\rightarrow A3,}$ (S28, S39 and S40) and $spt6_{S5\rightarrow A5}$ (S94, S13, S144, S155 and S206). As shown in Figure S2J, the $spt6_{S3\rightarrow A3}$ mutant was completely insensitive to 37°C and 200 mM HU,

whereas the *spt6*$_{S5\rightarrow A5}$ mutant showed intermediate sensitivity as compared with the *spt6*$_{S8\rightarrow A8}$ strain. These results imply that all eight identified CKII sites are required for the proper function of Spt6.

Because the turnover rate of Spt6 was increased in the *spt6*$_{S8\rightarrow A8}$ mutant, (Figure 1F), we also examined the steady-state protein levels generated from both the *spt6*$_{S8\rightarrow A8}$ and *spt6*$_{S8\rightarrow E8}$ mutants at permissive temperature and elevated temperatures at which the *spt6*$_{S8\rightarrow A8}$ mutant is lethal. Spt6 protein levels were similar to WT levels in both the *spt6*$_{S8\rightarrow A8}$ and *spt6*$_{S8\rightarrow E8}$ strains at the permissive temperature (Figure 1I, lanes 2-4). In contrast, at the restrictive temperature, we observed a partial decrease of Spt6 protein level in the *spt6*$_{S8\rightarrow A8}$, but not in the *spt6*$_{S8\rightarrow E8}$ mutant (Figure 1I, lanes 6-8). Consistent with a decrease in Spt6 levels, we also observed a subtle decrease in Set2 protein and a decrease in H3K36me3 levels in the *spt6*$_{S8\rightarrow A8}$ mutant at the restrictive temperature, in agreement with our initial findings that CKII inactivation affects H3K36me (Figure S1A).

CKII-Mediated Phosphorylation of Spt6 is Required for Proper Nucleosome Occupancy

We next sought to understand how CKII phosphorylation of Spt6 would impact its nucleosome deposition function. To this end, we performed ChIP-seq for histone H3 in our WT, *spt6*$_{S8\rightarrow A8}$ and *spt6*$_{S8\rightarrow E8}$ cells. Analysis of the histone levels across all genes in WT cells showed the distribution pattern of nucleosomes normally observed across gene bodies (Figures 2A and 2B). In sharp contrast, however, nucleosome occupancy in the *spt6*$_{S8\rightarrow A8}$ mutant strain (and to a lesser extent in the *spt6*$_{S8\rightarrow E8}$ strain) was significantly decreased at the 5'-ends of genes while nucleosomes levels increased at their 3'-ends (Figures 2A and 2B). Given nucleosome levels were depleted at 5'-ends of genes in the *spt6*$_{S8\rightarrow A8}$ mutant, we next asked if this might be correlated with changes in Spt6 occupancy. However, and as shown in Figures 2C and 2D, genome-wide Spt6 occupancy was not different between WT and the *spt6* mutants, indicating that the defects observed in

nucleosome occupancy at the 5'-ends of genes is not likely a result of CKII-mediated phosphorylation controlling Spt6's localization.

Although global occupancy of Spt6 was unaffected in the *spt6*$_{S8\rightarrow A8}$ mutant, further inspection of our Spt6 ChIP-seq dataset did in fact reveal that a subset of genes (n=316; most stringent cutoff) had decreased localization of Spt6 at the 5'-ends without a change at their 3'-ends (Figure S3A). As anticipated, histone levels across the same subset of 316 genes in the *spt6*$_{S8\rightarrow A8}$ mutant showed a corresponding nucleosome occupancy defect at the 5'-ends (Figure S3B), consistent with our global analysis of H3 levels (Figures 2A and 2B). These findings were validated by ChIP-qPCR at two example genes: one within the most stringent cut-off list of 316 genes (*TDH3*) and another just outside this list (*PMA1*) (see Figures S3E and S3F for localization of Spt6 and Figures S3G and S3H for the localization of H3). Further bioinformatic analysis of these 316 genes revealed that they were longer and more highly transcribed on average than the global average (Figures S3I and S3J, respectively). However, examination of the GO terms associated with this subset did not reveal any clear enrichment of pathways. As an additional control, we followed the same methodology to determine if there would be genes in which Spt6 was increased at the 5'-end, instead of a decrease. These analyses showed few examples for which Spt6 subtly increased at the 5'-ends in *spt6*$_{S8\rightarrow A8}$ cells, and, further, these genes showed no histone occupancy differences compared with WT cells. Bioinformatics analysis of these genes revealed that they were shorter (Figure S3K) and expressed at lower levels compared with the global average (Figure S3J, blue bars), suggesting that the subtle Spt6 increases were related to having lower levels of Spt6 at these genes leading to higher variance and noise. Collectively, these results reveal an important role for phosphorylation of Spt6 by CKII in nucleosome deposition.

CKII-dependent Phosphorylation of Spt6 Suppresses Antisense Transcription

Given the requirement of CKII-mediated phosphorylation of Spt6 in maintaining proper nucleosome occupancy, we next asked if CKII phosphorylation of Spt6 would be required to suppress antisense transcripts normally observed in mutants of *SPT6* (DeGennaro et al., 2013; Ivanovska et al., 2011; Kiely et al., 2011). To determine the effect of our *spt6* mutations on antisense transcription, we performed a stranded RNA-seq analysis (with spike-in controls for normalization) in our WT, $spt6_{S8\rightarrow A8}$, $spt6_{S8\rightarrow E8}$, and *spt6-1004* strains. The *spt6-1004* allele caused drastic changes in antisense transcription, a result consistent with previous studies (Figure 3A) (Cheung et al., 2008; Ivanovska et al., 2011). A comparison of antisense transcripts between the $spt6_{S8\rightarrow A8}$ *and* $spt6_{S8\rightarrow E8}$ mutants with the WT profile showed that, although the $spt6_{S8\rightarrow A8}$ mutant exhibited increased antisense transcription, the $spt6_{S8\rightarrow E8}$ mutant showed minimal change in antisense transcription (Figure 3A).

Closer inspection of our RNA-seq data sets for antisense transcripts showed us that there were 914 unique antisense transcripts in the *spt6-1004* mutant relative to WT (Figure 3B). The $spt6_{S8\rightarrow A8}$ strain also demonstrated an increase in the number of unique antisense transcripts relative to WT (52), and more than 50% of these transcripts overlapped with the unique antisense transcripts predicted in the *spt6-1004* mutant (34 out of 52) (Figure 3B). In stark contrast to the $spt6_{S8\rightarrow A8}$ mutant, the $spt6_{S8\rightarrow E8}$ mutant showed little to no unique antisense transcripts (Figures 3A and 3B). A heat map of the antisense transcripts originating from the *spt6-1004* allele and $spt6_{S8\rightarrow A8}$ mutant showed that the majority of antisense transcripts in the *spt6-1004* and $spt6_{S8\rightarrow A8}$ mutants originated from the 5'-ends of genes (Figures 3C-3G), which is where nucleosome occupancy was most affected by the absence of CKII phosphorylation of Spt6 (Figures 2A and Supplementary Figures 3G and 3H). Two examples of this finding are shown in Figures 3H and 3I, which show high levels of antisense transcription emerging from the 5'-ends of the *YTA6* and *SMY1* loci. The $spt6_{S8\rightarrow E8}$ and WT strains did not exhibit these high levels of antisense transcription (Figure 3H and 3I).

We further validated the occurrence of these antisense transcripts by strand-specific qRT-PCR and determined whether they would be associated with nucleosome decreases at their 5'-ends. As predicted, the levels of *YTA6* and *SMY1* antisense transcripts were elevated in *spt6-1004* and *spt6*$_{S8\rightarrow A8}$ mutants compared with WT (Figures S4A and S4B). The *spt6*$_{S8\rightarrow E8}$ strain showed a slight increase in the *YTA6* antisense transcript but no increase of the *SMY1* antisense transcript. Taken together, these observations reinforce the idea that phosphorylation of Spt6 by CKII plays an important role in the maintenance of chromatin structure at the 5'-ends of genes. These findings are also in agreement with Perales et al., that found that artificial depletion of Spt6 using a temperature degron (*td*) caused preferential loss of nucleosomes from the 5'-ends of genes (Perales et al., 2013).

CKII-dependent Phosphorylation of Spt6 is Required to Suppress Sense Cryptic Transcription and Maintain Genome Integrity

In addition to preventing antisense transcription, Spt6 is well known to suppress sense transcripts from arising from within the bodies of genes. We therefore next asked whether the inability of CKII to phosphorylate Spt6 would result in increased cryptic transcription similar that that observed for antisense transcription. To initially address this question, we examined two cryptic-prone genes, *STE11* and *SPB4* (Cheung et al., 2008) (Figures S5A and S5B) using a quantitative real-time polymerase chain reaction (qRT-PCR) method that can detect the presence of cryptic transcription arising from the sense direction (Dronamraju et al., 2018; Jeronimo et al., 2015). As shown previously, the *spt6-1004* cells (Figures S5C and S5D) and *spt6*$_{S8\rightarrow A8}$ (Figures S5E and S5F) cells showed a ~5-fold increase in the 3' RNA levels (i.e., cryptic transcription) arising at the *STE11* and *SPB4* loci. Our analyses also showed that the 5' to 3' RNA levels at these genes were unaffected in WT and the *spt6*$_{S8\rightarrow E8}$ cells (Figures S5E and S5F). Consistent with the production of sense cryptic transcription, ChIP-qPCR for H3 to monitor nucleosome occupancy

revealed a significant reduction in the levels of nucleosomes at the 3'-ends of the *STE11* and *SPB4* genes (68% and 72%) in the $spt6_{S8\rightarrow A8}$ mutant strain but not in the $spt6_{S8\rightarrow E8}$ mutant (Figures S5G and S5H).

The *SRG1-SER3* gene expression system is another well-established system to monitor the impact of chromatin integrity on proper gene transcription (Figure 4A) (Hainer et al., 2011; Martens et al., 2004; Martens et al., 2005). In the presence of serine, expression of *SRG1* causes transcriptional interference and repression of *SER3*. When serine is deprived, *SRG1* transcription is attenuated, which removes transcriptional interference and enables increased expression of *SER3*. However, mutation of factors that affect chromatin integrity, such as *SPT6*, causes de-repression of *SER3* independent of *SRG1* (due to the loss of nucleosome occupancy at the *SRG1* locus) (Nourani et al., 2006; Thebault et al., 2011). Therefore, we examined the potential of the $spt6_{S8\rightarrow A8}$ and $spt6_{S8\rightarrow E8}$ mutants to bypass the normal regulation of the *SRG1-SER3* system. As expected and consistent with the established role of Spt6 in maintaining *SER3* repression, we found that *SER3* levels were up-regulated in the *spt6-1004* allele and $spt6_{S8\rightarrow A8}$, whereas the level of de-repression was lower in the $spt6_{S8\rightarrow E8}$ mutant (Figure 4B). We confirmed the increase in the expression level of *SER3* in the *spt6-1004 and* $spt6_{S8\rightarrow A8}$ mutant by qRT-PCR (Figures 4C and 4D, respectively). As predicted from these findings, the $spt6_{S8\rightarrow A8}$ mutant caused a loss of nucleosome occupancy at *SRG1* locus (Figure 3E). Conversely, in the $spt6_{S8\rightarrow E8}$ mutant, both nucleosome occupancy at *SRG1* and increased *SER3* expression were largely unaffected. Further analysis of our RNA-seq data set showed broad sense transcription defects in the *spt6-1004* allele, although less so for the $spt6_{S8\rightarrow A8}$ mutant (Figure S6). These results show that CKII phosphorylation of Spt6 is required for nucleosome deposition and chromatin integrity thereby governing stringent control of gene transcription.

Spt6-Spn1 Interaction is Regulated by CKII-Dependent Phosphorylation of Spt6

Spt6 co-purifies with a variety of transcription-associated proteins, including histones, RNAPII, and Spn1. To determine which of these interactions, if any, would be affected by the absence of CKII phosphorylation of Spt6, we affinity purified FLAG-tagged Spt6 (n=4) and FLAG-tagged *spt6*$_{S8\rightarrow A8}$ (n=4) and subjected the purified complexes to mass spectrometry analysis (MS). Significance Analysis of Interactome (SAINT) analysis was performed to obtain protein-protein interaction probabilities for the MS results obtained from FLAG tagged strains relative to each other and untagged controls (n=4) . The association of Spn1 with Spt6 in the *spt6*$_{S8\rightarrow A8}$ mutant was reduced by ~50% compared with WT (Figure 5B), suggesting that Spn1 association with Spt6 is regulated by CKII phosphorylation of Spt6. Histone and RNAPII interactions with Spt6 were not disrupted by the loss of CKII phosphorylation (Figure 5B, Figure S7). A full list of the differential interactions identified is provided in Supplementary Table 6. In support of the MS results, the Spt6-Spn1 interaction was reduced in the *spt6*$_{S8\rightarrow A8}$ mutant strain without any significant effect in the *spt6*$_{S8\rightarrow E8}$ mutant by co-immunoprecipitation and immunoblot probing for Spn1 (Figure 5C). Finally, when we treated immunoprecipitated FLAG-Spt6 with lambda phosphatase prior to immunoblotting, the interaction with Spn1 decreased significantly, a result that further confirmed the phospho-dependence of the Spt6-Spn1 interaction (Figure 5D).

Because phosphorylation of Spt6 by CKII is required for the proper Spt6-Spn1 interaction, we next asked whether mutations in *SPN1* that perturb its interactions with Spt6 (e.g., *spn1-R263D* and *spn1-F267E*) phenocopy the *spt6*$_{S8\rightarrow A8}$ mutant. As shown in Figure S8A, these *spn1* mutants showed a decrease in H3K36 methylation, RNAPII Ser2 CTD phosphorylation, and sickness at 37°C and on 200 mM HU plates (Figure S8B). In addition, we found that these *spn1* mutants, like *spt6*$_{S8\rightarrow A8}$ (Figures 4B and 4C), caused de-repression of *SER3* in the *SRG1-SER3* model (Figure S7C). A similar result occurred when we used a mutation in Spt6 that perturbs Spn1 interaction (*spt6-F249K*) (Figure S8C). Based on these findings, we created a double mutant of *spt6*$_{S8\rightarrow A8}$ with *spn1-R263D* to examine the consequence of combining orthogonal

mutants that impair Spt6-Spn1 interaction. Strikingly, this double mutant was synthetically sick under normal growth conditions, and it was lethal either at 37°C or in the presence of 200 mM HU (Figure 5E). These findings agree with observations by McDonald et al., who examined orthogonal mutants of Spt6 and Spn1 that disrupt Spn1-Spt6 interaction (i.e., *spt6-F249K* + *spn1-F267E* and *spt6-F249K* + *spn1-R263D*) (McDonald et al. 2010). Finally, further examination of this double mutant revealed decreases in H3K36 methylation and RNAPII levels, suggesting that the interaction between Spt6 and Spn1 is also crucial for Spt6-Ctk1-Set2 regulation (Figure 5F).

DISCUSSION

Spt6 deposits nucleosomes in the wake of elongating RNAPII, and a lack of functional Spt6 causes open chromatin regions (Cheung et al., 2008; Ivanovska et al., 2011); however, the mechanisms that regulate Spt6 function are largely unknown. Although multiple enzymes associate with RNAPII during transcription initiation/elongation, the activities of these enzymes on the full RNAPII elongation complex have not been fully explored. Here we show that CKII, phosphorylates Spt6 to enforce nucleosome reassembly and chromatin stability that are required for proper transcriptional regulation. Using SILAC-based mass spectrometry, we confirmed that Spt6 is phosphorylated by CKII at multiple N-terminal sites, a region of Spt6 that interacts with histones and Spn1 (McCullough et al., 2015; McDonald et al., 2010). Further, we establish that Spt6 phosphorylation by CKII is important for proper nucleosome occupancy of nearly all RNAPII transcribed genes and find this role to be particularly important at the 5'-ends of genes. Consistent with this finding, mutants of *spt6* that cannot be phosphorylated show elevated levels of antisense transcription originating from the 5'-ends of genes. Mechanistically, we show that Spt6 phosphorylation is required for proper Spt6-Spn1 interaction, which we suggest plays a role in regulating the ability of Spt6 to deposit nucleosomes and enforce directionality of RNAPII, as represented in Figure 6.

A major observation from our study is the role CKII-dependent phosphorylation of Spt6 plays in regulating the global balance of nucleosomes along genes. Our studies found that prevention of Spt6 phosphorylation by CKII leads to depletion of histone H3 (a proxy for nucleosome occupancy) at the 5'-ends of genes with a corresponding increase in H3 at their 3'-ends (Figure 2A and 2B). The global decrease of nucleosomes we observed may be due to the fact that phosphorylated Spt6, and the stabilized interaction of Spn1 it directs, is important for 5-end nucleosome reassembly during transcription. In the absence of phosphorylated Spt6, nucleosomes appear to buildup at the 3'-end due to RNAPII transcription moving and thereby compacting nucleosomes towards the 3'-ends of genes. Another possibility that is not mutually exclusive with the idea above, is that phosphorylated Spt6 maintains nucleosomes at the 5'-ends by recruiting/activating the machinery that prevents active histone exchange. One such mechanism that prevents histone exchange is Set2, whose function is intertwined with the presence of functional Spt6. Indeed, our results show that CKII-dependent phosphorylation of Spt6 affects Set2-dependent H3K36 methylation (Figures S1A and 1I). Consistent with the loss of nucleosomes in the *spt6*$_{S8\rightarrow A8}$ mutant at the 5'-ends, we also observed an increase in sense and antisense cryptic transcription, which was more pronounced at the 5'-ends of genes.

It is important to also note that while this work was in revision, Gouot *et al.* also reported that Spt6 is phosphorylated by CKII, and they showed that this phosphorylation contributes to the suppression of cryptic transcription (Gouot et al., 2018). The authors showed that the increase in cryptic transcription was attributed to an increase in histone exchange in *ck2-ts* and in *spt6* mutants that cannot be phosphorylated, a result that is consistent with our findings of the *spt6*$_{S8\rightarrow A8}$ mutant having nucleosome occupancy changes. Thus, there is large agreement between these two studies.

One key mechanistic finding of our study is the importance of CKII phosphorylation in maintaining Spt6-Spn1 interaction. Spn1 (IWS1 in higher metazoans) is a binding partner of Spt6,

and, heretofore, we did not suspect the existence of a mechanism that maintains the association or the broad effects of Spt6-Spn1 heterodimerization on chromatin (Fischbeck et al., 2002; Krogan et al., 2002). Because Spn1 binding occurs in close proximity to the N-terminal CKII phosphorylation sites, we hypothesized that Spn1 binding to Spt6 is regulated or fine-tuned by CKII phosphorylation. It may be that an increased acidity of N-terminal phosphorylated Spt6 promotes Spn1 binding, or alternatively Spt6 phosphorylation may eliminate an intra-molecular inhibitory interaction to make the Spn1 binding site accessible. Although proof of such an autoinhibitory mechanism is beyond the scope of this study, such a mechanism exists for other histone chaperones, such as Spt2 and HJURP, that are modified post-translationally to release inhibitory states to regulate histone binding (Warren and Shechter, 2017). Interestingly, Li *et al.* also showed that full-length Spn1 interacts with DNA, histone H3/H4, mononucleosomes, and nucleosomal arrays, and Spn1 has a weak nucleosome deposition activity (Li et al., 2018). Thus, phosphorylation-mediated interaction of Spn1 with the Spt6 N-terminus could have effects on the overall function of Spt6, partly mediated by the decreased stability and its ability to interact with RNAPII or other factors.

In addition to regulating Spt6-Spn1 association, CKII phosphorylation of Spt6 may affect chromatin integrity by affecting the interaction between Spt6 and Spt2 (Bhat et al., 2013). However, we have not found any effect of deletion of *SPT2* on Set2/H3K36me levels (unpublished results), indicating that the effects of the *ck2-ts* mutation on Spt6, Set2, and H3K36me levels are not simply due to the absence of Spt6-Spt2 interaction. In addition, our extensive MS analyses and co-immunoprecipitation experiments showed that the $spt6_{S8\rightarrow A8}$ mutation did not affect the ability of Spt6 to interact with RNAPII (Figure S7). Thus, the major consequence of CKII phosphorylation of Spt6 is to maintain Spn1 association. Future studies are required to precisely determine the mechanistic basis of this interaction and how it contributes to nucleosome reassembly.

Finally, it is important to mention that the function of CKII in transcriptional regulation and chromatin maintenance is likely to be highly conserved. Other investigators have documented an important function of CKII in transcriptional regulation from yeast to humans (Basnet et al., 2014), and the N-terminus of human Spt6 (SUPT6H) has similar consensus CKII phosphorylation sites that are phosphorylated (summarized at www.phosphosite.org). Thus, it will be exciting to determine the extent to which CKII phosphorylation of SUPT6H broadly contributes to chromatin reassembly and transcriptional fidelity during gene transcription.

ACCESSION NUMBERS

The GEO accession number for the RNA-seq datasets reported in this paper is The accession number for the RNaseq and ChIPseq data reported in this paper is GEO: GSE122620. Raw data for immunoblots can be found at https://data.mendeley.com/datasets/zzc659t39m/draft?a=50b72eec-60d5-4b24-ba6c-e1e0938f4fd4.

AUTHOR CONTRIBUTIONS

RD and BDS conceived the ideas and designed the experiments with input from ALM and JLK. RD, JLK, KDH, and SAP performed the experiments with technical help from DP and SA. RD and BDS wrote the manuscript.

ACKNOWLEDGMENTS

We sincerely thank the members of the Strahl, Davis, and Mosley labs for critical discussions and comments, and Howard Fried for editorial suggestions. We thank David Glover for the *ck2* temperature sensitive mutant strains. We also thank the UNC high-throughput sequencing facility for their support. BDS acknowledges support from NIH grant GM126900, and IJD acknowledges

support from NIH grants CA166447 and CA198482 and the Corn-Hammond Fund for Pediatric Oncology. ALM acknowledges support from NSF grant MCB 1515748.

FUNDING SOURCES

This work was supported by a NIH grant (GM126900) to BDS and an NSF grant (1515748) to ALM. JLK was supported by NIH F32-GM116352 and a postdoctoral fellowship awarded by University of North Carolina Lineberger Comprehensive Cancer Center Basic Mechanisms of Viral and Chemical Carcinogenesis Training Grant 5 T32 CA009156.

FIGURE LEGENDS

Figure 1. CKII phosphorylation of the N-terminus of Spt6 is essential for Spt6 function. (A) Schematic representation of the Spt6 domain organization. Eight consensus CKII phosphorylation sites are indicated in a magnified version of the Spt6 N-terminus. (B) Schematic representation of SILAC experimental approach. (C) Differential abundance analysis of Spt6 peptides identified by SILAC and MS1 quantitation (n=1). Peptides containing CKII consensus sites are indicated by the colors defined in the legend. The asterisks represent=*, abundance ratios were adjusted to an artifical minimum value due to detection in WT only; **, abundance ratios were adjusted to a maximum value due to detection in *ck2 ts* only.(D) In vitro CKII kinase assay using bacterially expressed, N-terminal 6X HIS-tagged Spt6 fragments (1-300, WT and mutant). Shown are the Coomassie staining (extreme left), anti-6X-HIS immunoblotting (middle panel) and γ^{32}P-ATP radioactivity incorporation using the recombinant, commercially purified CKII enzyme (right). Data shown are representative images of three biological replicates. (E) Left panel shows a silver stained SDS-PAGE gel of load levels for FLAG-Spt6 affinity purified from yeast, both WT and *spt6*$_{S8\rightarrow A8}$ mutant prior to kinase and ^{32}P-ATPγ addition. Right panel shows an autoradiograph of *in vitro* CKII kinase assay using the same affinity purified FLAG-Spt6. CKII auto-phosphorylation is also indicated.(F) Immunoblots using anti-FLAG antibody to detect FLAG-Spt6 from WT and *spt6*$_{S8\rightarrow A8}$ mutant cells after treatment with 200 μg/ml of cycloheximide to inhibit protein translation. Cell lysates were prepared as described in Materials and Methods. G6PDH was used as a loading control. Immunoblot experiments are representative images from three biological replicates. (G) Spotting assay showing the growth and sensitivity of *spt6* and *ck2-ts* mutants at 37 ºC and under conditions of genotoxic stress [200 mM hydroxyurea (HU)]. (H) Growth and sensitivity of the putative CKII phospho-mutants *spt6*$_{S8\rightarrow A8}$ and phospho-mimic *spt6*$_{S8\rightarrow E8}$ as assessed in panel E. For panels G and H, the yeast spotting assays were repeated three times with three individual colonies and images shown are representative of the data (I) Immunoblot analysis of the changes in the levels of Spt6, Set2, and H3K36me3 in asynchronously growing cultures of control (WT untagged Spt6 and WT FLAG-Spt6) and *spt6* mutants (*spt6*$_{S8\rightarrow A8}$ and *spt6*$_{S8\rightarrow E8}$) at 30ºC and 37ºC. H3 and G6PDH levels were used as loading controls. Immunoblot experiments were repeated three times and the images shown are representative examples from three biological replicates.

Figure 2. CKII-dependent phosphorylation of Spt6 maintains nucleosome occupancy at the 5'-ends of genes. (A) Heat map of global changes in H3 occupancy rank ordered by gene expression frequency in WT, *spt6*$_{S8\rightarrow A8}$ and *spt6*$_{S8\rightarrow E8}$ cells. (B) Metagene analysis of H3 occupancy as depicted by a line plot in WT, *spt6*$_{S8\rightarrow A8}$ and *spt6*$_{S8\rightarrow E8}$ cells. (C) Heat map showing Spt6 occupancy genome-wide rank ordered by gene expression frequency in WT, *spt6*$_{S8\rightarrow A8}$ and *spt6*$_{S8\rightarrow E8}$ cells. (D) Metagene analysis of ChIP-seq of Spt6 as depicted by line plots in WT, *spt6*$_{S8\rightarrow A8}$ and *spt6*$_{S8\rightarrow E8}$ cells.

Figure 3. Spt6 phosphorylation by CKII is required to prevent antisense transcription. (A) Stranded RNA-seq was performed as described in Materials and Methods; the panel shows the changes in the antisense transcripts in the mutants of *spt6* over the WT, *spt6*$_{S8\rightarrow A8}$, and *spt6*$_{S8\rightarrow E8}$ *and spt6-1004* allele. (B) Venn diagram showing the distribution of antisense transcripts in WT, *spt6*$_{S8\rightarrow A8}$, and *spt6*$_{S8\rightarrow E8}$ *and spt6-1004* mutants. Numbers in the circles represent the unique number of antisense transcripts generated in the respective mutant. (C) Heatmap of antisense RNA-seq signal (black). 971 differential antisense transcripts were predicted between WT and *spt6-1004*, coinciding with 829 genes. *spt6-1004* antisense RNA-seq signal ($\log_2$) was plotted across the 829 genes. The subplot in the top right highlights 40 genes coinciding with differential antisense transcripts predicted between WT and *spt6*$_{S8\rightarrow A8}$ (C; wheat=outside of gene body, white-black = $\log_2$ antisense signal). (D) Antisense levels of the highlighted 40 genes between the 5' and 3' halves were compared. The 5' half of the genes had significantly more antisense signal than the 3' half ($p < 0.0001$, Wilcoxon rank-sum). (E) On a per gene basis, the 5' and 3' half ratios ($\log_2$) were plotted. While not every gene had higher 5' signal relative to the 3' half of the genes (8), 80% (or 32 genes) did. (F) Antisense levels of all 829 genes were compared between the 5' and 3' halves of the genes. Like the 40 highlighted genes, the 5' halves had significantly more antisense signal relative to the 3' halves ($p < 0.0001$, Wilcoxon rank-sum). (G) The 5' and 3' half

ratios were calculated for each of the 829 genes and plotted. 80.6% (668) of the genes had higher signal in the 5' half of the gene while 19.4% (161) had higher antisense signal in the 3' half of the gene. (H) and (I) are representative UCSC genome browser tracks of *SMY1* and *YTA6* genes selected from the RNA-seq data set.

Figure 4. CKII phosphorylation of Spt6 regulates chromatin integrity during transcription. (A) Schematic of the *SRG1* and *SER3* loci showing their expression pattern in WT and mutant strains as indicated by red (WT) and green (mutant) arrows. (B) Representative RNA-seq tracks showing an increase in the expression level of the *SER3* gene in WT, $spt6_{S8\rightarrow A8}$, $spt6_{S8\rightarrow E8}$, and *spt6-1004* allele. (C) qRT-PCR detection of *SRG1* and *SER3* transcripts in the WT and *spt6-1004* mutant strain. (D) qRT-PCR detection of *SRG1* and *SER3* transcripts in the WT and *spt6* mutant ($spt6_{S8\rightarrow A8}$ and $spt6_{S8\rightarrow E8}$) strains. (E) ChIP analysis of histone H3 levels across *SRG1* and *SER3* was performed with WT and *spt6* mutant ($spt6_{S8\rightarrow A8}$ and $spt6_{S8\rightarrow E8}$) strains. Amplicons are indicated below the schematic diagram of the genes. qRT-PCR and ChIP data are represented as mean ± SD of three independent biological experiments. Asterisks indicate significance values (** $p<0.01$); non-significant comparisons are not shown. All qPCR primer sequences (B-D) are listed in Supplementary Table S4.

Figure 5. Spt6-Spn1 interaction is dependent on CKII phosphorylation of Spt6. FLAG-tagged Spt6 was affinity purified from WT and $spt6_{S8\rightarrow A8}$ mutant cells using FLAG-M2 agarose beads, and the protein was subjected to MS analyses. (A) Correlation plot analysis of the bait normalized fold change values (*100) for FLAG Spt6 isolated from the WT and $spt6_{S8\rightarrow A8}$ mutant. The red diamond indicates Spn1. (B) Relative levels of indicated proteins in the $spt6_{S8\rightarrow A8}$ mutant compared with WT. (C) Co-IP showing the interaction of Spt6 and Spn1. Spn1 was immunoprecipitated by anti-V5 antibody and Spt6 was detected using anti-FLAG antibody. (D)

Interaction of Spt6 and Spn1 is phospho-dependent. Lysates were prepared from WT cells expressing FLAG-Spt6 and V5-tagged Spn1. Spt6 was immobilized on FLAG-M2 agarose beads, and the complex was treated with lambda phosphatase. Immunoblots were performed for Spt6 and Spn1 after two washes. Co-IPs were performed three times and the immunoblots shown are representative images of these experiments. (E) Spotting assay showing the growth and sensitivity of single mutants of *spt6 and spn1* (top panel) and double mutants of *spn1* mutant (*spn1-R263D*) and $spt6_{S8\rightarrow A8}$ at 37ºC and under conditions of genotoxic stress 200 mM hydroxyurea (HU). All spotting assays were performed three independent times with independent colonies; shown are representative images. (F) Immunoblots showing the changes in the levels of Spt6, RNAPII, H3 and H3K36me3 in the single and double mutants of *spn1-R263D* and $spt6_{S8\rightarrow A8}$. All immunoblots were performed three independent times using independent clones.

Figure 6. A model for CKII-mediated control of Spt6 function during transcription. During transcription, CKII phosphorylates Spt6 within its N-terminus, promoting Spn1 association and proper nucleosome reassembly that prevents inappropriate transcription from within gene bodies. If Spt6 is not phosphorylated, Spn1 interaction is reduced, causing defects in Spt6 and RNAPII localization, and nucleosome deposition defects that permit cryptic sense and antisense transcription.

SUPPLEMENTARY FIGURE LEGENDS

Supplementary Figure 1. CKII interacts with Spt6 and regulates histone post-translational modifications. (A) Immunoblot showing methylation levels on histone H3 in WT and *ck2-ts* strains at permissive (30°C) and non-permissive (25°C and 37°C) temperatures. Total H3 levels were used as a loading control. (B) Co-immunoprecipitation of Spt6 and CKII. Extracts of yeast strains with endogenously epitope-tagged Spt6 (FLAG) and untagged CKII, tagged CKA1 (6HA), or tagged CKA2 (6HA) were immunoprecipitated with FLAG antibody (see Methods). Samples

were immunoblotted with HA antibody to assess the Spt6:CKII interaction. RNAPII CTD-S2phos immunoblot is shown as a positive control for interaction with Spt6. FLAG and G6PDH immunoblots are shown for additional controls. All experiments were performed in triplicate and the images shown are representative examples of the replicates.

Supplementary Figure 2. Representative MS/MS spectra for the eight CKII phosphorylation sites within the N-terminus of Spt6. (A-H) MS/MS fragment spectra are shown with relative fragment ion intensity on the y-axis and mass to charge ratio (m/z) on the x-axis. The y-ion series is in blue and the b-ion series is in red as annotated by SEQUEST HT and visualized in Scaffold 4 software. Neutral loss data are in green. The related amino acid information for each ion series is shown at the top of each panel. (I) Immunoblots showing degradation kinetics of $spt6_{S8\rightarrow E8}$ protein in the mutant stain using cycloheximide chase assay. Cells were treated with 100 μg/ml of CHX and lysates were prepared as described in materials and methods and subjected to immunoblot analysis (J) Spotting assay showing the growth and sensitivity of *WT,* $spt6_{S3\rightarrow A3}$*,* $spt6_{S5\rightarrow A5}$*, and* $spt6_{S8\rightarrow A8}$ mutants at 37ºC and under conditions of genotoxic stress [200 mM hydroxyurea (HU)]. Immunoblots and spotting assays shown are representative images from three biological replicates.

Supplementary Figure 3. CKII phosphorylation-dependent Spt6 distribution is impacted on long and highly transcribed genes. (A) and (B) Metagene plots of Spt6 (A) and H3 (B) in WT (black lines) $spt6_{S8\rightarrow A8}$ (red lines) and $spt6_{S8\rightarrow E8}$ (blue lines) aligned to the transcription start site (TSS) of a subset of genes (n=316). (C) and (D) are schematic representation of *PMA1* and *TDH3*, respectively, with the primer sets approximate locations. (E) and (F) ChIP-qPCR analysis of Spt6 at the *PMA1* and *TDH3* loci in the indicated WT and $spt6_{S8\rightarrow A8}$ and $spt6_{S8\rightarrow E8}$ mutants. (G and H) ChIP-qPCR analysis of H3 at the *PMA1* and *TDH3* loci in the indicated WT and $spt6_{S8\rightarrow A8}$ and $spt6_{S8\rightarrow E8}$ mutants. All ChIP-qPCR data are represented as mean ± standard deviation of three

biological replicates (n=3) and * p<0.05, ** p<0.01as assessed by Student's t test. (I) Histogram of length distribution of genes that show a decrease is the localization of Spt6 and H3 at the 5'-ends of genes in *spt6*$_{S8\rightarrow A8}$. mutant compared to the WT cells (J) A histogram showing genes that tend to have a decrease in the levels of Spt6 and H3 at the 5'-ends genes in the *spt6*$_{S8\rightarrow A8}$ mutant (compared to the 3'-ends) tend to be highly expressed (red histograms) than the global average. (K) Histogram showing the distribution of gene length in a set of control genes (where Spt6 levels were higher at the 5'-ends) compared to all the genes.

Supplementary Figure 4. RT-qPCR validation of antisense transcription in mutants of *spt6*. (A) qRT-PCR detection of *YTA6* transcript in the WT, *spt6*$_{S8\rightarrow A8}$, *spt6*$_{S8\rightarrow E8}$, and *spt6-1004* strains. (B) qRT-PCR detection of *SMY1* transcript in the WT, *spt6*$_{S8\rightarrow A8}$, *spt6*$_{S8\rightarrow E8}$, and *spt6-1004* strains. Data are represented as mean ± SD of three biological experiments, and significance was determined using Student's t-test. ** indicate p<0.01, *** indicate p<0.001 and ****p<0.0001 and non-significant comparisons represented by n.s. All primer sequences are listed in Supplementary Table S4.

Supplementary Figure 5. CKII-dependent Spt6 phosphorylation is required for maintenance of chromatin integrity. (A) and (B) Diagram of the *STE11* and *SPB4* loci. Arrows indicate the main transcript and potential cryptic transcripts arising from within the respective gene bodies. Black and gray bars underneath the loci represent the 5' and the 3' amplicons, which are detected by qRT-PCR as a measure of cryptic transcription (C) and (D). (C) and (D) qRT-PCR detection of the 5' and the 3' amplicons at the *STE11* (E) and *SPB4* (F) loci, respectively in the WT or *spt6-1004* mutant yeast strains grown at permissive (30ºC) or non-permissive (37ºC) temperatures. (E) and (F) qRT-PCR detection of the 5' and the 3' amplicons at the *STE11* and *SPB4* loci in WT or *spt6* mutant (*spt6*$_{S8\rightarrow A8}$ and *spt6*$_{S8\rightarrow E8}$) strains. (G) and (H) ChIP showing

changes in the nucleosome occupancy levels at the promoters and open reading frames (ORF) of *STE11* and *SPB4,* respectively in WT or *spt6* mutant (*spt6*$_{S8\rightarrow A8}$ and *spt6*$_{S8\rightarrow E8}$) strains. qRT-PCR and ChIP data are represented as mean ± SD of three independent biological experiments, and significance was determined using a Student's t test. Asterisks indicate significance values, where *p<0.05, **p<0.01; non-significant comparisons are not shown. All qPCR primer sequences (C-I) are listed in Supplementary Table S4.

Supplementary Figure 6. CKII phosphorylation of Spt6 is required for proper global gene transcription. Stranded RNA-seq was performed using three biological replicates as described in Materials and Methods and shown are the changes in the sense transcripts in the mutants of Spt6 over the WT, *spt6*$_{S8\rightarrow A8}$, and *spt6*$_{S8\rightarrow E8}$ and *spt6-1004* strains. The red dots signify the genes that are either up or down-regulated in the *spt6-1004* allele compared to the WT.

Supplementary Figure 7. Spt6 interaction with RNAPII is independent of CKII phosphorylation of Spt6. Co-immunoprecipitation of *spt6* mutants with RNAPII. Yeast strains with endogenously FLAG-tagged Spt6 (WT, *spt6*$_{S8\rightarrow A8}$, or *spt6*$_{S8\rightarrow E8}$) were lysed and immunoprecipitated with FLAG antibody (see Methods). Samples were immunoblotted with RNAPII antibody to assess changes in the interaction. Co-IPs were performed in triplicate and representative images are shown.

Supplementary Figure 8. Spt6-Spn1 interaction is required for transcription and histone methylation. (A) Immunoblots showing changes in marks associated with transcription and histone methylation. (B) Spotting assays showing the requirements of Spt6-Spn1 interactions for resistance to heat and genotoxic agents. (C) qRT-PCR detection of *SRG1* and *SER3* transcripts in the WT and *spt6-F249K, spn1-R263D* and *spn1-F267E* mutant strains. qRT-PCR data are represented as mean ± SD of three independent biological experiments, and significance was

determined using a Student's t test. Asterisks indicate significance values, where *p<0.05, **p<0.01; non-significant comparisons are not shown. All qPCR primer sequences are listed in Supplementary Table S4.

REFERENCES

Ahn, S.H., Keogh, M.C., and Buratowski, S. (2009). Ctk1 promotes dissociation of basal transcription factors from elongating RNA polymerase II. EMBO J *28*, 205-212.

Andrulis, E.D., Werner, J., Nazarian, A., Erdjument-Bromage, H., Tempst, P., and Lis, J.T. (2002). The RNA processing exosome is linked to elongating RNA polymerase II in Drosophila. Nature *420*, 837-841.

Basnet, H., Su, X.B., Tan, Y., Meisenhelder, J., Merkurjev, D., Ohgi, K.A., Hunter, T., Pillus, L., and Rosenfeld, M.G. (2014). Tyrosine phosphorylation of histone H2A by CK2 regulates transcriptional elongation. Nature *516*, 267-271.

Bedard, L.G., Dronamraju, R., Kerschner, J.L., Hunter, G.O., Axley, E.D., Boyd, A.K., Strahl, B.D., and Mosley, A.L. (2016). Quantitative Analysis of Dynamic Protein Interactions during Transcription Reveals a Role for Casein Kinase II in Polymerase-associated Factor (PAF) Complex Phosphorylation and Regulation of Histone H2B Monoubiquitylation. J Biol Chem *291*, 13410-13420.

Bhat, W., Boutin, G., Rufiange, A., and Nourani, A. (2013). Casein kinase 2 associates with the yeast chromatin reassembly factor Spt2/Sin1 to regulate its function in the repression of spurious transcription. Mol Cell Biol *33*, 4198-4211.

Bortvin, A., and Winston, F. (1996). Evidence that Spt6p controls chromatin structure by a direct interaction with histones. Science *272*, 1473-1476.

Chapman, R.D., Palancade, B., Lang, A., Bensaude, O., and Eick, D. (2004). The last CTD repeat of the mammalian RNA polymerase II large subunit is important for its stability. Nucleic Acids Res *32*, 35-44.

Cheung, V., Chua, G., Batada, N.N., Landry, C.R., Michnick, S.W., Hughes, T.R., and Winston, F. (2008). Chromatin- and transcription-related factors repress transcription from within coding regions throughout the Saccharomyces cerevisiae genome. PLoS Biol *6*, e277.

Close, D., Johnson, S.J., Sdano, M.A., McDonald, S.M., Robinson, H., Formosa, T., and Hill, C.P. (2011). Crystal structures of the S. cerevisiae Spt6 core and C-terminal tandem SH2 domain. J Mol Biol *408*, 697-713.

Collart, M.A., and Oliviero, S. (2001). Preparation of yeast RNA. Curr Protoc Mol Biol *Chapter 13*, Unit13 12.

Cui, P., Jin, H., Vutukuru, M.R., and Kaplan, C.D. (2016). Relationships Between RNA Polymerase II Activity and Spt Elongation Factors to Spt- Phenotype and Growth in Saccharomyces cerevisiae. G3 (Bethesda) *6*, 2489-2504.

de Godoy, L.M. (2014). SILAC yeast: from labeling to comprehensive proteome quantification. Methods Mol Biol *1156*, 81-109.

DeGennaro, C.M., Alver, B.H., Marguerat, S., Stepanova, E., Davis, C.P., Bahler, J., Park, P.J., and Winston, F. (2013). Spt6 regulates intragenic and antisense transcription, nucleosome positioning, and histone modifications genome-wide in fission yeast. Mol Cell Biol *33*, 4779-4792.

Dejean, Y. (1970). [Prognosis and treatment of essential facial paralysis]. Cah Med *11*, 1273-1282.

Dengl, S., Mayer, A., Sun, M., and Cramer, P. (2009). Structure and in vivo requirement of the yeast Spt6 SH2 domain. J Mol Biol *389*, 211-225.

Diebold, M.L., Koch, M., Loeliger, E., Cura, V., Winston, F., Cavarelli, J., and Romier, C. (2010a). The structure of an Iws1/Spt6 complex reveals an interaction domain conserved in TFIIS, Elongin A and Med26. EMBO J *29*, 3979-3991.

Diebold, M.L., Loeliger, E., Koch, M., Winston, F., Cavarelli, J., and Romier, C. (2010b). Noncanonical tandem SH2 enables interaction of elongation factor Spt6 with RNA polymerase II. J Biol Chem *285*, 38389-38398.

Dobin, A., Davis, C.A., Schlesinger, F., Drenkow, J., Zaleski, C., Jha, S., Batut, P., Chaisson, M., and Gingeras, T.R. (2013). STAR: ultrafast universal RNA-seq aligner. Bioinformatics *29*, 15-21.

Dronamraju, R., Hepperla, A.J., Shibata, Y., Adams, A.T., Magnuson, T., Davis, I.J., and Strahl, B.D. (2018). Spt6 Association with RNA Polymerase II Directs mRNA Turnover During Transcription. Mol Cell *70*, 1054-1066 e1054.

Dronamraju, R., and Strahl, B.D. (2014). A feed forward circuit comprising Spt6, Ctk1 and PAF regulates Pol II CTD phosphorylation and transcription elongation. Nucleic Acids Res *42*, 870-881.

Eitoku, M., Sato, L., Senda, T., and Horikoshi, M. (2008). Histone chaperones: 30 years from isolation to elucidation of the mechanisms of nucleosome assembly and disassembly. Cell Mol Life Sci *65*, 414-444.

Endoh, M., Zhu, W., Hasegawa, J., Watanabe, H., Kim, D.K., Aida, M., Inukai, N., Narita, T., Yamada, T., Furuya, A*., et al.* (2004). Human Spt6 stimulates transcription elongation by RNA polymerase II in vitro. Mol Cell Biol *24*, 3324-3336.

Erdel, F., and Rippe, K. (2011). Chromatin remodelling in mammalian cells by ISWI-type complexes--where, when and why? FEBS J *278*, 3608-3618.

Fischbeck, J.A., Kraemer, S.M., and Stargell, L.A. (2002). SPN1, a conserved gene identified by suppression of a postrecruitment-defective yeast TATA-binding protein mutant. Genetics *162*, 1605-1616.

Formosa, T. (2003). Changing the DNA landscape: putting a SPN on chromatin. Curr Top Microbiol Immunol *274*, 171-201.

Gelbart, M.E., Rechsteiner, T., Richmond, T.J., and Tsukiyama, T. (2001). Interactions of Isw2 chromatin remodeling complex with nucleosomal arrays: analyses using recombinant yeast histones and immobilized templates. Mol Cell Biol *21*, 2098-2106.

Gouot, E., Bhat, W., Rufiange, A., Fournier, E., Paquet, E., and Nourani, A. (2018). Casein kinase 2 mediated phosphorylation of Spt6 modulates histone dynamics and regulates spurious transcription. Nucleic Acids Res.

Hainer, S.J., Pruneski, J.A., Mitchell, R.D., Monteverde, R.M., and Martens, J.A. (2011). Intergenic transcription causes repression by directing nucleosome assembly. Genes Dev *25*, 29-40.

Hanna, D.E., Rethinaswamy, A., and Glover, C.V. (1995). Casein kinase II is required for cell cycle progression during G1 and G2/M in Saccharomyces cerevisiae. J Biol Chem *270*, 25905-25914.

Hartzog, G.A., Wada, T., Handa, H., and Winston, F. (1998). Evidence that Spt4, Spt5, and Spt6 control transcription elongation by RNA polymerase II in Saccharomyces cerevisiae. Genes Dev *12*, 357-369.

Ho, L., and Crabtree, G.R. (2010). Chromatin remodelling during development. Nature *463*, 474-484.

Hockman, D.J., and Schultz, M.C. (1996). Casein kinase II is required for efficient transcription by RNA polymerase III. Mol Cell Biol *16*, 892-898.

Ivanovska, I., Jacques, P.E., Rando, O.J., Robert, F., and Winston, F. (2011). Control of chromatin structure by spt6: different consequences in coding and regulatory regions. Mol Cell Biol *31*, 531-541.

Janke, C., Magiera, M.M., Rathfelder, N., Taxis, C., Reber, S., Maekawa, H., Moreno-Borchart, A., Doenges, G., Schwob, E., Schiebel, E.*, et al.* (2004). A versatile toolbox for PCR-based tagging of yeast genes: new fluorescent proteins, more markers and promoter substitution cassettes. Yeast *21*, 947-962.

Jeronimo, C., and Robert, F. (2016). Histone chaperones FACT and Spt6 prevent histone variants from turning into histone deviants. Bioessays *38*, 420-426.

Jeronimo, C., Watanabe, S., Kaplan, C.D., Peterson, C.L., and Robert, F. (2015). The Histone Chaperones FACT and Spt6 Restrict H2A.Z from Intragenic Locations. Mol Cell *58*, 1113-1123.

Kaplan, C.D., Holland, M.J., and Winston, F. (2005). Interaction between transcription elongation factors and mRNA 3'-end formation at the Saccharomyces cerevisiae GAL10-GAL7 locus. J Biol Chem *280*, 913-922.

Kent, W.J., Zweig, A.S., Barber, G., Hinrichs, A.S., and Karolchik, D. (2010). BigWig and BigBed: enabling browsing of large distributed datasets. Bioinformatics *26*, 2204-2207.

Keogh, M.C., Kim, J.A., Downey, M., Fillingham, J., Chowdhury, D., Harrison, J.C., Onishi, M., Datta, N., Galicia, S., Emili, A.*, et al.* (2006a). A phosphatase complex that dephosphorylates gammaH2AX regulates DNA damage checkpoint recovery. Nature *439*, 497-501.

Keogh, M.C., Mennella, T.A., Sawa, C., Berthelet, S., Krogan, N.J., Wolek, A., Podolny, V., Carpenter, L.R., Greenblatt, J.F., Baetz, K.*, et al.* (2006b). The Saccharomyces cerevisiae histone H2A variant Htz1 is acetylated by NuA4. Genes Dev *20*, 660-665.

Kiely, C.M., Marguerat, S., Garcia, J.F., Madhani, H.D., Bahler, J., and Winston, F. (2011). Spt6 is required for heterochromatic silencing in the fission yeast Schizosaccharomyces pombe. Mol Cell Biol *31*, 4193-4204.

Krogan, N.J., Kim, M., Ahn, S.H., Zhong, G., Kobor, M.S., Cagney, G., Emili, A., Shilatifard, A., Buratowski, S., and Greenblatt, J.F. (2002). RNA polymerase II elongation factors of Saccharomyces cerevisiae: a targeted proteomics approach. Mol Cell Biol *22*, 6979-6992.

Kurat, C.F., Lambert, J.P., van Dyk, D., Tsui, K., van Bakel, H., Kaluarachchi, S., Friesen, H., Kainth, P., Nislow, C., Figeys, D.*, et al.* (2011). Restriction of histone gene transcription to S phase by phosphorylation of a chromatin boundary protein. Genes Dev *25*, 2489-2501.

Kwak, H., and Lis, J.T. (2013). Control of transcriptional elongation. Annu Rev Genet *47*, 483-508.

Lai, A.Y., and Wade, P.A. (2011). Cancer biology and NuRD: a multifaceted chromatin remodelling complex. Nat Rev Cancer *11*, 588-596.

Li, H., Handsaker, B., Wysoker, A., Fennell, T., Ruan, J., Homer, N., Marth, G., Abecasis, G., Durbin, R., and Genome Project Data Processing, S. (2009). The Sequence Alignment/Map format and SAMtools. Bioinformatics *25*, 2078-2079.

Li, S., Almeida, A.R., Radebaugh, C.A., Zhang, L., Chen, X., Huang, L., Thurston, A.K., Kalashnikova, A.A., Hansen, J.C., Luger, K.*, et al.* (2018). The elongation factor Spn1 is a multi-functional chromatin binding protein. Nucleic Acids Res *46*, 2321-2334.

Liu, J., Zhang, J., Gong, Q., Xiong, P., Huang, H., Wu, B., Lu, G., Wu, J., and Shi, Y. (2011). Solution structure of tandem SH2 domains from Spt6 protein and their binding to the phosphorylated RNA polymerase II C-terminal domain. J Biol Chem *286*, 29218-29226.

Livak, K.J., Wills, Q.F., Tipping, A.J., Datta, K., Mittal, R., Goldson, A.J., Sexton, D.W., and Holmes, C.C. (2013). Methods for qPCR gene expression profiling applied to 1440 lymphoblastoid single cells. Methods *59*, 71-79.

Love, M.I., Huber, W., and Anders, S. (2014). Moderated estimation of fold change and dispersion for RNA-seq data with DESeq2. Genome Biol *15*, 550.

Martens, J.A., Laprade, L., and Winston, F. (2004). Intergenic transcription is required to repress the Saccharomyces cerevisiae SER3 gene. Nature *429*, 571-574.

Martens, J.A., Wu, P.Y., and Winston, F. (2005). Regulation of an intergenic transcript controls adjacent gene transcription in Saccharomyces cerevisiae. Genes Dev *19*, 2695-2704.

Martin, M. (2011). Cutadapt removes adapter sequences from high-throughput sequencing reads. 2011 *17*.

Mayer, A., Heidemann, M., Lidschreiber, M., Schreieck, A., Sun, M., Hintermair, C., Kremmer, E., Eick, D., and Cramer, P. (2012). CTD tyrosine phosphorylation impairs termination factor recruitment to RNA polymerase II. Science *336*, 1723-1725.

McCullough, L., Connell, Z., Petersen, C., and Formosa, T. (2015). The Abundant Histone Chaperones Spt6 and FACT Collaborate to Assemble, Inspect, and Maintain Chromatin Structure in Saccharomyces cerevisiae. Genetics *201*, 1031-1045.

McDonald, S.M., Close, D., Xin, H., Formosa, T., and Hill, C.P. (2010). Structure and biological importance of the Spn1-Spt6 interaction, and its regulatory role in nucleosome binding. Mol Cell *40*, 725-735.

Moqtaderi, Z., Yale, J.D., Struhl, K., and Buratowski, S. (1996). Yeast homologues of higher eukaryotic TFIID subunits. Proc Natl Acad Sci U S A *93*, 14654-14658.

Mosley, A.L., Sardiu, M.E., Pattenden, S.G., Workman, J.L., Florens, L., and Washburn, M.P. (2011). Highly reproducible label free quantitative proteomic analysis of RNA polymerase complexes. Mol Cell Proteomics *10*, M110 000687.

Nourani, A., Robert, F., and Winston, F. (2006). Evidence that Spt2/Sin1, an HMG-like factor, plays roles in transcription elongation, chromatin structure, and genome stability in Saccharomyces cerevisiae. Mol Cell Biol *26*, 1496-1509.

Patro, R., Duggal, G., Love, M.I., Irizarry, R.A., and Kingsford, C. (2017). Salmon provides fast and bias-aware quantification of transcript expression. Nat Methods *14*, 417-419.

Perales, R., Erickson, B., Zhang, L., Kim, H., Valiquett, E., and Bentley, D. (2013). Gene promoters dictate histone occupancy within genes. EMBO J *32*, 2645-2656.

Quinlan, A.R., and Hall, I.M. (2010). BEDTools: a flexible suite of utilities for comparing genomic features. Bioinformatics *26*, 841-842.

Ramirez, F., Ryan, D.P., Gruning, B., Bhardwaj, V., Kilpert, F., Richter, A.S., Heyne, S., Dundar, F., and Manke, T. (2016). deepTools2: a next generation web server for deep-sequencing data analysis. Nucleic Acids Res *44*, W160-165.

Sdano, M.A., Fulcher, J.M., Palani, S., Chandrasekharan, M.B., Parnell, T.J., Whitby, F.G., Formosa, T., and Hill, C.P. (2017). A novel SH2 recognition mechanism recruits Spt6 to the doubly phosphorylated RNA polymerase II linker at sites of transcription. Elife *6*.

Sun, M., Lariviere, L., Dengl, S., Mayer, A., and Cramer, P. (2010). A tandem SH2 domain in transcription elongation factor Spt6 binds the phosphorylated RNA polymerase II C-terminal repeat domain (CTD). J Biol Chem *285*, 41597-41603.

Svejstrup, J.Q. (2003). Transcription. Histones face the FACT. Science *301*, 1053-1055.

Thebault, P., Boutin, G., Bhat, W., Rufiange, A., Martens, J., and Nourani, A. (2011). Transcription regulation by the noncoding RNA SRG1 requires Spt2-dependent chromatin deposition in the wake of RNA polymerase II. Mol Cell Biol *31*, 1288-1300.

Warren, C., and Shechter, D. (2017). Fly Fishing for Histones: Catch and Release by Histone Chaperone Intrinsically Disordered Regions and Acidic Stretches. J Mol Biol *429*, 2401-2426.

Wilson, B.G., and Roberts, C.W. (2011). SWI/SNF nucleosome remodellers and cancer. Nat Rev Cancer *11*, 481-492.

Winston, F. (2001). Control of eukaryotic transcription elongation. Genome Biol *2*, REVIEWS1006.

Yoh, S.M., Cho, H., Pickle, L., Evans, R.M., and Jones, K.A. (2007). The Spt6 SH2 domain binds Ser2-P RNAPII to direct Iws1-dependent mRNA splicing and export. Genes Dev *21*, 160-174.

Youdell, M.L., Kizer, K.O., Kisseleva-Romanova, E., Fuchs, S.M., Duro, E., Strahl, B.D., and Mellor, J. (2008). Roles for Ctk1 and Spt6 in regulating the different methylation states of histone H3 lysine 36. Mol Cell Biol *28*, 4915-4926.

Zhang, L., Fletcher, A.G., Cheung, V., Winston, F., and Stargell, L.A. (2008). Spn1 regulates the recruitment of Spt6 and the Swi/Snf complex during transcriptional activation by RNA polymerase II. Mol Cell Biol *28*, 1393-1403.

STAR METHODS

CONTACT FOR REAGENT AND RESOURCE SHARING

Further information and requests for resources and reagents should be directed to, and will be fulfilled by, the Lead Contact, Brian D. Strahl (brian_stral@med.unc.edu).

EXPERIMENTAL MODEL AND SUBJECT DETAILS

All yeast strains are listed in Supplementary Table 2. Gene deletions and C-terminal epitope tagging of endogenous genes were performed by gene replacement (Gelbart et al., 2001; Janke et al., 2004). Plasmids used in this study are listed in Supplementary Table 2. Mutagenesis of pRS306-FLAG-SPT6, a gift from Fred Winston, Harvard Medical School, Boston, MA, (Kaplan et al., 2005) (Supplementary Table S2) was performed with the QuikChange Lightning Multi Site-

Directed Mutagenesis Kit (Agilent Technologies) and primers described in Supplementary Table 4. Plasmids were verified by Sanger sequencing prior to transformation of yeast by a standard two-step gene replacement method. All yeast strains were verified by PCR amplification of genomic DNA, Sanger sequencing, and immunoblotting for epitope-tagged proteins (primers are listed in Supplementary Table 3 and antibodies are described below).

METHOD DETAILS

SILAC methodology

WT Spt6-3XFLAG strains were cultured in complete minimal medium containing L-Lysine ($^{13}C_6$, $^{15}N_2$) and L-Arginine ($^{13}C_6$, $^{15}N_4$), which produce +8 and +10 dalton mass shifts, respectively. CKII mutant strains were cultured in complete minimal medium with light amino acids (specifically L-Lysine ($^{12}C_6$, $^{14}N_2$) and L-Arginine ($^{12}C_6$, $^{14}N_4$). Following cell pelleting and washing, cells were mixed at a 1:1 (wt/mutant) ratio and resuspended in TAP lysis buffer. Lysis was performed as described (Bedard et al., 2016). Purification efficiency was assessed by silver staining a TGX SDS-PAGE gel (Bio-Rad) prior to trichloroacetic acid precipitation of the Spt6-FLAG elutions. Protein pellets were resuspended in 8 M urea in 100 mM Tris-HCl (pH 8.5). Proteolytic digestions were performed with LysC-Trypsin Gold (Promega), quenched, and pressure loaded onto a three-phase multidimensional protein identification technology (MudPIT) column (Mosley et al., 2011). Samples were analyzed by 10-step MudPIT on an Orbitrap Fusion Lumos mass spectrometer. Two technical replicate analyses were performed with either collision induced dissociation based fragmentation or a combination of higher energy collision dissociation (HCD) and electron transfer dissociation with supplemental HCD activation. The resulting raw data were searched using SEQUEST HT in Proteome Discoverer 2.1 (Thermo) and quantitation was performed using built-in SILAC 8,10 quantitation mode for MS1 precursor intensity based quantitation.

Affinity-purification

Spt6-FLAG purifications from WT, mutant, or parental cells were performed as previously described from 6 L of asynchronous log phase grown yeast (Bedard et al., 2016). Following cryolysis, clarification, and incubation with anti-FLAG M2 agarose beads (Sigma-Aldrich); the beads were extensively washed with TAP lysis buffer before purified protein elution through incubation with a 10-fold excess of 3X FLAG peptide. Samples were digested with trypsin as described above and then analyzed by 10-step MudPIT on a Velos Pro Orbitrap mass spectrometer. Following database search against a yeast Uniprot fasta database, peptide-spectrum matches were used for SAINT analysis as previously described (Bedard et al., 2016). Co-immunoprecipitations were performed as described (Moqtaderi et al., 1996) with minor modifications. Overnight saturated yeast cultures were inoculated into 100 mL fresh YPD at an optical density 600 (OD_{600}) of about 0.2. Cells were grown to an OD_{600} of approximately 1-1.2, washed with water, and suspended in buffer containing 450 mM Tris-acetate (pH 7.8), 150 mM potassium acetate, 60% (v/v) glycerol, 3 mM EDTA (pH 8.0), and supplemented fresh with 3 mM DTT, 1 mM PMSF, 1X complete EDTA-free protease inhibitors (Roche). Suspended cells were lysed with glass beads using a mini bead beater (Disruptor Genei) for 10 minutes at 4°C, with 1 minute on and 1 minute off cycle in the cold room after which cells were allowed to rest for 10 minutes at 4°C, and then cleared by centrifugation for 15 minutes 4°C. Protein concentrations of lysates were estimated using a Bradford Protein Assay (Bio-Rad). One mg of total protein was incubated in 1 ml of buffer A [50 mM HEPES-KOH (pH 7.5), 1 mM EDTA (pH 8.0), 20% (v/v) glycerol, 125 mM potassium acetate, 1% (v/v) NP-40, supplemented fresh with 100 mM DTT] containing 30 µl of anti-FLAG M2 agarose (Sigma-Aldrich) overnight at 4°C. Next day, beads were washed 5 times in buffer A and protein complexes were eluted using 3X-FLAG peptide (Sigma) following the manufacturer's instructions. Proteins were separated by SDS-PAGE and subjected to immunoblotting to detect interacting proteins (antibodies are listed below). To study phospho-dependent interactions, FLAG-Spt6-bound beads were treated with 200 U of lambda phosphatase

for 30 minutes at 30°C. After incubation, beads were washed twice with buffer A and heated at 95°C in SDS loading buffer. For every co-immunoprecipitation, 10% input was applied to the gels.

Recombinant Spt6 and Spn1 expression and purification

The N terminal fragments of WT, *spt6*$_{S8\rightarrow A8}$ mutants (aa1-300) and structured region of Spn1 (aa 141-405) were cloned in *pET28a* as 6X-HIS tagged fragments. Plasmids were sequenced to confirm the orientation and the existence of *spt6*$_{S8\rightarrow A8}$ mutation before progressing with purification. Recombinant proteins were purified as described elsewhere. Briefly, plasmids were transformed into SoluBL21 cells and log phase cultures of bacteria were induced with 1mM IPTG at 16°C overnight. Next day, cells were centrifuged and lysates were prepared in lysis buffer (50 mM NaH_2PO_4, 300 mM NaCl, 20 mM imidazole, pH to 8.0, 1 mg/ml Lysozyme, 2 microL/ml Universal Nuclease and 1% Triton X100) containing 20 mM imidazole and applied to Ni-NTA agarose columns. Lysate was incubated with beads for 2h at 4°C and subjected to six washes with wash buffer (50 mM NaH_2PO_4, 300 mM NaCl, 20 mM imidazole, pH to 8.0). Proteins were eluted in wash buffer containing 300mM imidazole and dialyzed overnight in wash buffer containing 20 mM imidazole. Protein concentrations were estimated using Bradford reagent.

In vitro Kinase Assays

In vitro kinase assays were performed as described previously (Bedard et al., 2016). Briefly, the bacterially expressed and purified fragments of Spt6 and the full length Spt6 purified from asynchronously growing yeast cells was incubated either alone or with 500 Units of CKII enzyme. The reactions were carried out in the kinase buffer (40 mM HEPES [pH 7.5], 10 mM MgCl2, 5 mM dithiothreitol, and 10 µCi of [γ-32P]-ATP) (6000Ci/mmol; Perkin Elmer) for 2hrs at 30°C. Reactions were stopped by adding SDS-PAGE loading buffer. Samples were boiled for 10 minutes and subjected to SDS-PAGE, dried, and exposed to film for autoradiography.

Cycloheximide Chase Assays

Cycloheximide chase assays were performed to ascertain the turnover of Spt6 in the WT and *spt6*$_{S8\rightarrow A8}$ mutants as described previously (Dronamraju and Strahl, 2014). Briefly, strains were grown in a special synthetic complete (SC) media that contained 0.1% proline as a source of nitrogen. Yeast strains of indicated genotypes grown overnight were diluted to an OD_{600} of 0.2 and allowed to grow until they reached an OD_{600} of 1 in the presence of 0.003% SDS. Cells were collected at various time points and fixed and lysed in 10% trichloroacetic acid (TCA as described elsewhere (Keogh et al., 2006a; Keogh et al., 2006b). Proteins were separated by SDS-PAGE and immunoblotted using antibodies specific for indicated proteins.

Immunoblotting

Yeast strains of the indicated genotypes (and their wild-type counterparts) were grown in YPD either at permissive or restrictive temperatures. Overnight-saturated cultures were diluted to an OD_{600} of 0.2 and allowed to grow until they reached an OD_{600} of 1. Five OD_{600} equivalents of cells were lysed using a modified TCA extraction method as described (Keogh et al., 2006a; Keogh et al., 2006b). 10-20 µg of the lysates were separated by SDS-PAGE and variously probed with the following antibodies: anti-FLAG-M2 [for FLAG tagged Spt6] (Sigma-Aldrich, F1804; 1:5000), anti-G6PDH (Sigma-Aldrich, A9521; 1:100,000), anti-histone H3K4me3 (EpiCypher, 13-0004; 1:5000), anti-histone H3K79me3 (Abcam, ab2651, 1:2500) anti-histone H3K36me3 (Abcam, ab9050, ab9050; 1:1000), anti-histone H3 (EpiCypher, 13-0001; 1:50,000), anti-Spt16 (gift from Tim Formosa University of Utah, 1:5000), anti-H3K36me2 (Active Motif, 39255; 1:1000), anti-Set2 (Generated in the Strahl lab, 1:5000), anti-RNAPII-Ser2P (Active Motif, Clone #3E10, 61084; 1:100), anti-H2BK123ub1 (Cell Signaling Technology, 5546; 1:2000), and anti-H2B (Active Motif, 39237; 1:2000). HRP-conjugated anti-rabbit (GE Healthcare, NA934V; 1:10,000) and anti-mouse

secondary (GE Healthcare, NA931V; 1:10,000), antibodies were used at 1:1000 and proteins were detected using ECL Prime or enhanced chemiluminescence ECL (Amersham Biosciences).

Spotting assays

Spotting assays were used to assess the sensitivities of the yeast strains to drugs and temperature changes. Saturated yeast cultures of the indicated genotypes were diluted to an OD_{600} of 0.2, followed by a five-fold serial dilution, and spotted on plates with or without 200 mM hydroxyurea (HU). Growth was assessed after 3 days at 30°C or 37°C. Every experiment was performed at least three times and the representative images are shown.

RNA extraction and real-time quantitative PCR

Yeast cell RNA was extracted using a hot acid phenol method (Collart and Oliviero, 2001). The isolated RNA was treated with 10 U of RNAse-free DNAse (Promega) for 30 minutes, followed by RNA cleanup (Qiagen RNeasy Mini Kit, 74106). cDNA was synthesized from one µg of total RNA using random hexamer primers and Superscript Reverse Transcriptase III (Thermo-Fisher Scientific, 108-80044). The cDNA was diluted 1:25 before being subjected to real-time PCR (primers shown in Supplementary Table 4). Quantitative real-time PCR was performed using the SYBR Green Master mix according to manufacturer's instructions (Bio-Rad, 1725270), and the relative quantities of transcripts were calculated using the $\Delta\Delta C_t$ method (Livak et al., 2013) and *ACT1* or *PGK1* as controls. The data shown are the replicates of three independent experiments with three technical replicates in each experiment, and the significance values were calculated using Fisher t-test.

Chromatin immunoprecipitation

ChIP was performed as described with modifications (Ahn et al., 2009). The DNA from the pull-downs was estimated using quantitative real time PCR (primers described in Supplementary

Table 3). Data are mean of % input values +/- the standard deviations from three biological replicates with three technical replicates in each experiment. Significance values were calculated using Fisher t-test.

RNA-seq methodology and Data Analysis

RNA was extracted using acid-phenol method (Collart and Oliviero, 2001) and was quantified spectrophotometrically. 2.5μg of total RNA was used to deplete rRNA using the Ribo-zero kit (Illumina). ERCC spike-in controls were added to the RNA samples after rRNA clean-up and before proceeding on to the library preparation. Stranded RNA-seq libraries were prepared using TruSeq Stranded Total RNA sample preparation according to manufacturer's instructions. The libraries were sequenced on Illumina HiSeq 2500, paired-end 50bp reads). RNA-seq reads were first trimmed for possible adapter contamination using cutadapt (v1.10), (Martin, 2011) with the recommended sequence for Illumina adapters as well as a minimum read length of 36 base pairs (bp). Low quality reads were then filtered with fastq_quality_filter, a function within the fastx-toolkit (v0.0.14), with command line options -p 90 and -q 20 to keep reads with at least a 20 Phred score at a minimum of 90% of the bases. Reads were then aligned to the sacCer3 genome using STAR (v2.5.2b), (Dobin et al., 2013) and the following options: --quantMode TranscriptomeSAM, --outFilterMismatchNmax 2, --alignIntronMax 1000000, --alignIntronMin 20, --chimSegmentMin 15, --chimJunctionOverhangMin 15, --outSAMtype BAM Unsorted, --outFilterType BySJout, --outFilterScoreMin 1, and --outFilterMultimapNmax 1. A GTF file was given for the --sjdbGTFfile option that was generated in house combining the sacCer3 RefSeq and ERCC spike-in GTFs. Finally, the Salmon (v0.8.1), (Patro et al., 2017) function quant was used to quantify RNA counts over each gene, and DESeq2 (v1.14.1), (Love et al., 2014) was used to calculate differential genes.

Stranded RNA-seq allows us to map reads to specific strands, so all aligned reads were assigned sense or antisense based on whether they overlapped sacCer3 RefSeq genes in the

same or opposite strand, respectively. Reads that didn't overlap any gene were discarded for any stranded analyses as we couldn't confidently assign them sense/antisense. Unfortunately, overlapping genes cause reads to be assigned to both sense and antisense, so regions of gene overlap plus 49bp on either side (to account for read length) were subtracted out using bedtools (v2.26), (Quinlan and Hall, 2010), and expression of the remaining regions was re-quantified and run through DESeq2 to determine differential genes. Antisense cryptic transcripts were identified using previously published methods with no changes except using a minimum of 0.5 RPKM versus their previous minimum of 4.0 FPKM (Dejean, 1970). File conversions were done with samtools (v1.3.1, (Li et al., 2009)) and in-house scripts.

Reads were initially aligned and processed as paired end fragments, however signal tracks demonstrated an unusual pile-up of reads at specific and consistent locations across the gene that only occurred in the "R1" reads. To eliminate potential biases this may have added to downstream analyses, we only used the "R2" reads in this work. As no global transcriptional changes were observed using the ERCC spike-in, ERCC reads were removed from the dataset and not used for downstream analysis or quantification.

ChIP-seq methodology and Data Analysis

ChIP-seq reads were first trimmed for possible adapter contamination using cutadapt (v1.10), (Martin, 2011) with the recommended sequence for Illumina adapters as well as a minimum read length of 36 base pairs (bp). Low quality reads were then filtered with fastq_quality_filter, a function within the fastx-toolkit (v0.0.14), with command line options -p 90 and -q 20 to keep reads with at least a 20 Phred score at a minimum of 90% of the bases. To eliminate possible PCR artifacts from library preparation, we used in-house scripts to keep at most 5 reads that had the same sequence, where those above that threshold were filtered out. As this was paired end sequencing, we used in-house scripts to re-synchronize the reads that were kept into proper, ordered pairs between "R1" and "R2" fastqs for alignment. Reads were then aligned to the

sacCer3 genome using STAR (v2.5.2b), (Dobin et al., 2013) and the following options: --outFilterMultimapNmax 1, --outFilterMismatchNmax 2, --chimSegmentMin 15, --chimJunctionOverhangMin 15, --outSAMtype BAM Unsorted, --outFilterType BySJout, --outFilterScoreMin 1, and --outFilterMultimapNmax 1. The sacCer3 RefSeq GTF file was given for the option --sjdbGTFfile. Samtools (v1.3.1) (Li et al., 2009) was used to eliminate alignments that did not contain properly paired reads or were not primary alignments. Bigwigs were then made using genomeCov within bedtools (v2.26), (Quinlan and Hall, 2010) as well as tool bedGrapthToBigWig (Kent et al., 2010).

To identify genes that had low 5' levels of Spt6 ChIP-seq signal in *spt6*$_{S8\rightarrow A8}$ relative to WT, we calculated the $\log_2$ ratio of average signal between the first and second half of each gene for both *spt6*$_{S8\rightarrow A8}$ and WT. The variance of this score was calculated across three replicates, and genes with variance >0.01 for either *spt6*$_{S8\rightarrow A8}$ or WT were removed to select genes with consistent signal across replicates. For the remaining genes, the difference of ratios between *spt6*$_{S8\rightarrow A8}$ and WT were calculated (i.e., $log2\left(\frac{avg(WT\ first\ half\ signal)}{avg(WT\ second\ half\ signal)}\right) - log2\left(\frac{avg(S8A\ first\ half\ signal)}{avg(S8A\ second\ half\ signal)}\right)$). Those with a score of 0.15 or greater were selected for downstream analyses.

Once these genes were selected, Deeptools (v2.5.4) (Ramirez et al., 2016) tool computeMatrix in scale-region mode was used to make metagene plots about these genes for both H3 and Spt6 ChIP-seqs. Options included -b 200, -a 200, -bs 1, and -m 1000.

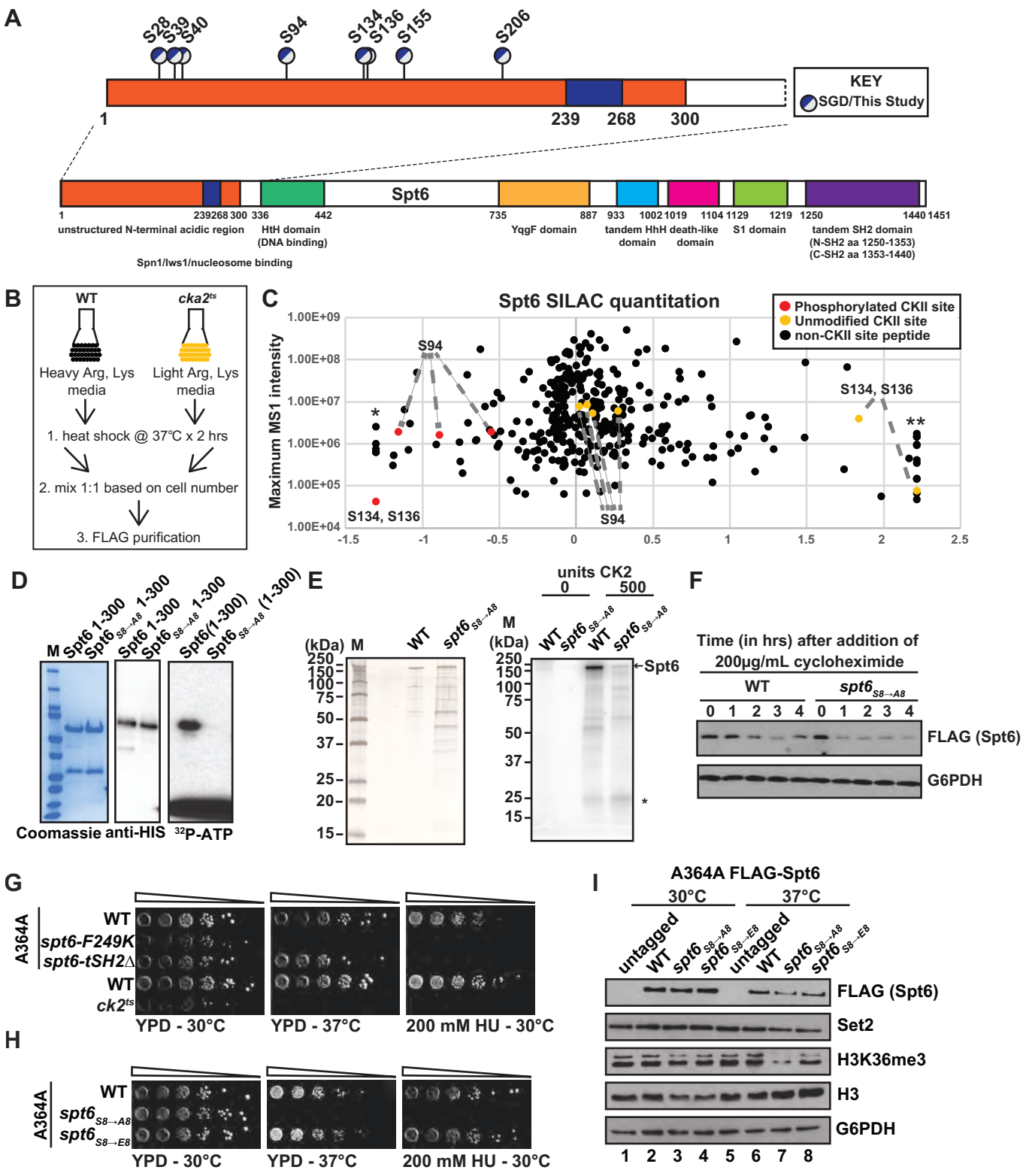
A
S28
S39
S40
S94
S134
S136
S155
S206
KEY
SGD/This Study
1
239
268
300
Spt6
1
239268 300
336
442
735
887
933
1002 1019
1104 1129
1219
1250
1440 1451
unstructured N-terminal acidic region
HtH domain
(DNA binding)
Spn1/lws1/nucleosome binding
YqgF domain
tandem HhH
domain
death-like
domain
S1 domain
tandem SH2 domain
(N-SH2 aa 1250-1353)
(C-SH2 aa 1353-1440)
B
WT
cka2ts
Heavy Arg, Lys media
Light Arg, Lys media
1. heat shock @ 37°C x 2 hrs
2. mix 1:1 based on cell number
3. FLAG purification
C
Spt6 SILAC quantitation
Phosphorylated CKII site
Unmodified CKII site
non-CKII site peptide
Maximum MS1 intensity
S94
S134, S136
S134, S136
S94
D
M
Spt6 1-300
Spt6 S8→A8 1-300
Spt6 1-300
Spt6 S8→A8 1-300
Spt6(1-300)
Spt6 S8→A8 (1-300)
Coomassie
anti-HIS
32P-ATP
E
units CK2
0
500
(kDa)
M
WT
spt6 S8→A8
Spt6
F
Time (in hrs) after addition of 200µg/mL cycloheximide
WT
spt6 S8→A8
0 1 2 3 4 0 1 2 3 4
FLAG (Spt6)
G6PDH
G
A364A
WT
spt6-F249K
spt6-tSH2Δ
WT
ck2ts
YPD - 30°C
YPD - 37°C
200 mM HU - 30°C
H
A364A
WT
spt6 S8→A8
spt6 S8→E8
YPD - 30°C
YPD - 37°C
200 mM HU - 30°C
I
A364A FLAG-Spt6
30°C
37°C
untagged
WT
spt6 S8→A8
spt6 S8→E8
FLAG (Spt6)
Set2
H3K36me3
H3
G6PDH
1 2 3 4 5 6 7 8

Figure 1

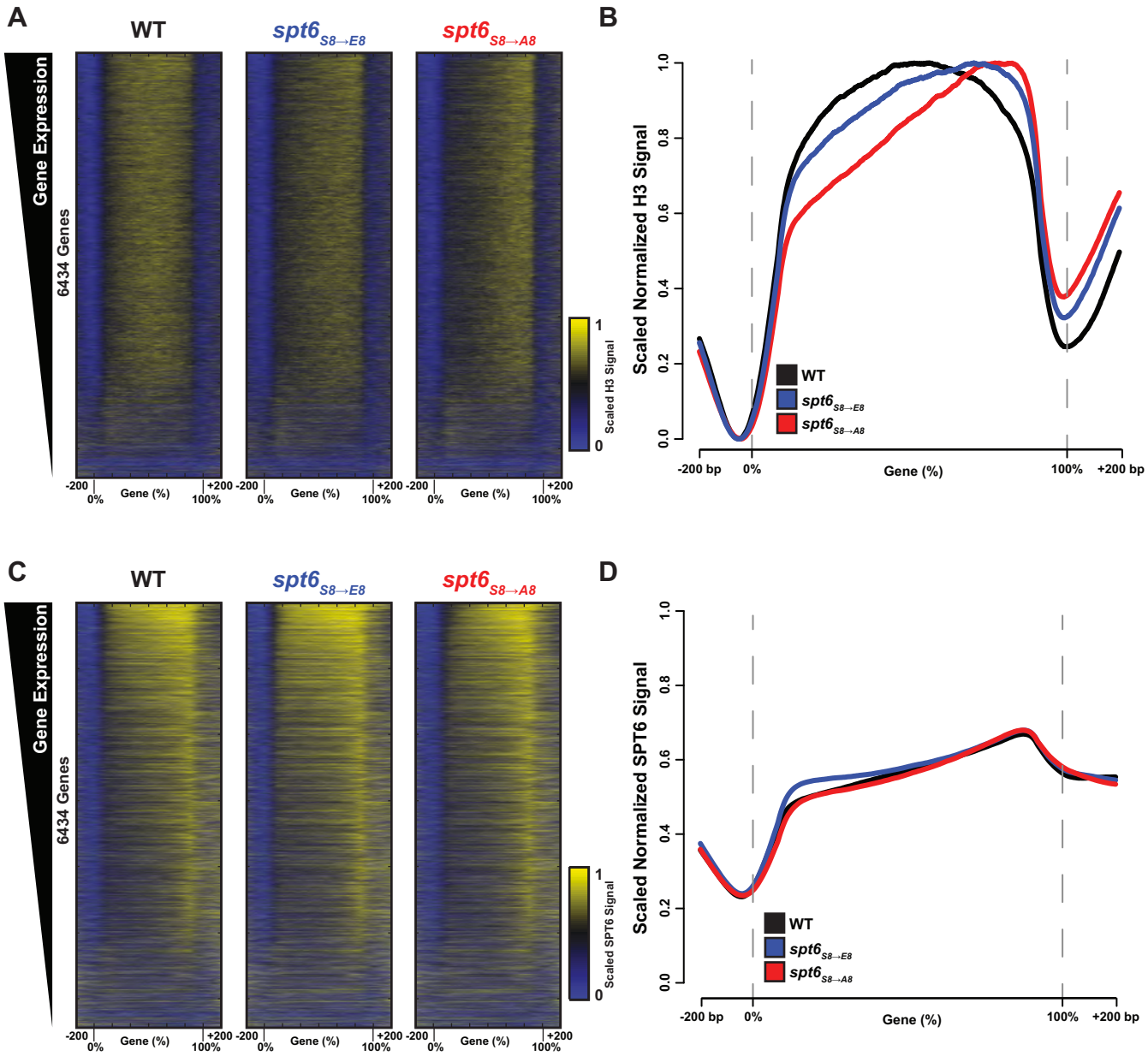
A
WT
spt6S8→E8
spt6S8→A8
Gene Expression
6434 Genes
-200
0%
Gene (%)
+200
100%
1
0
Scaled H3 Signal
B
Scaled Normalized H3 Signal
1.0
0.8
0.6
0.4
0.2
0.0
WT
spt6S8→E8
spt6S8→A8
-200 bp
0%
Gene (%)
100%
+200 bp
C
WT
spt6S8→E8
spt6S8→A8
Gene Expression
6434 Genes
-200
0%
Gene (%)
+200
100%
1
0
Scaled SPT6 Signal
D
Scaled Normalized SPT6 Signal
1.0
0.8
0.6
0.4
0.2
0.0
WT
spt6S8→E8
spt6S8→A8
-200 bp
0%
Gene (%)
100%
+200 bp

Figure 2

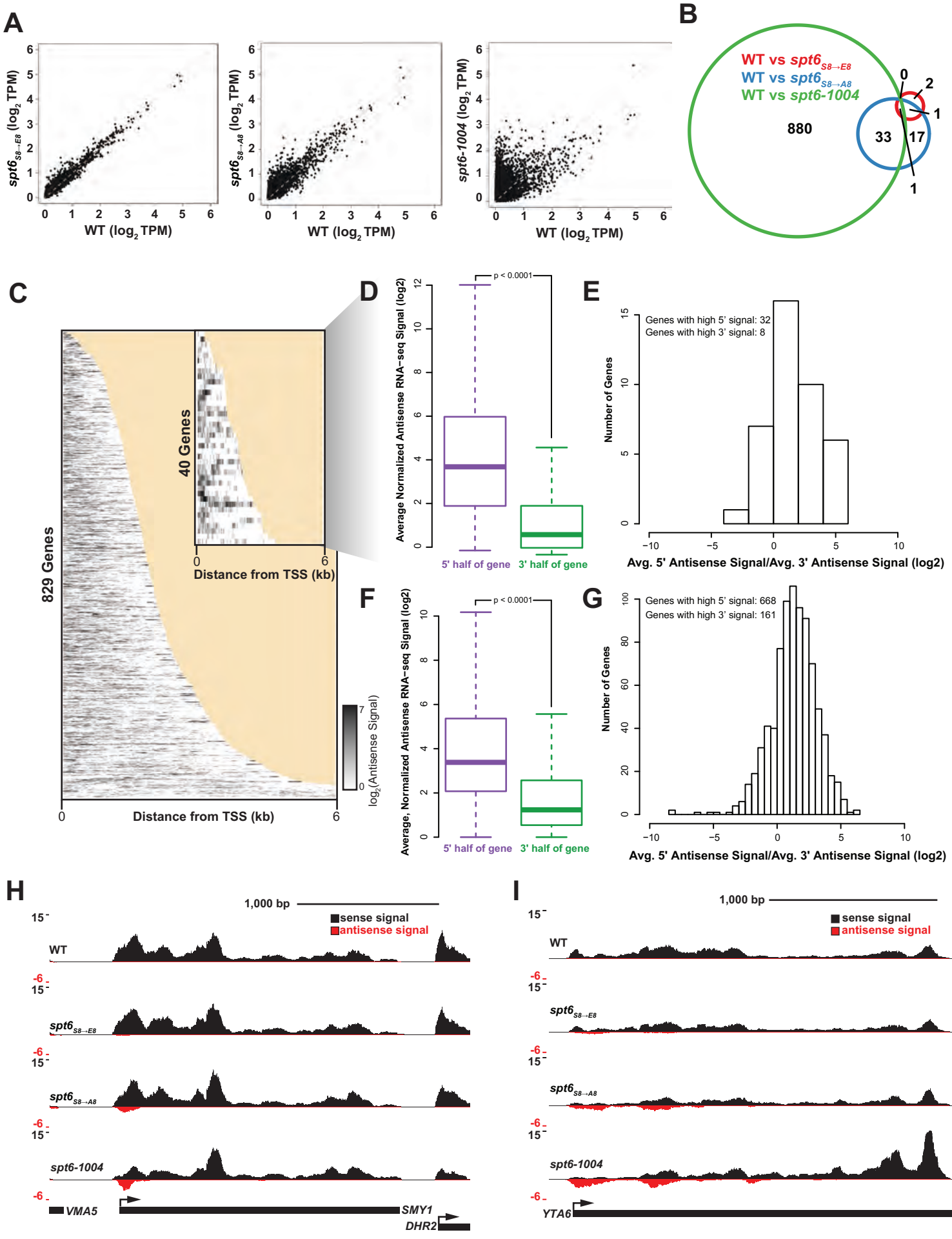
A
spt6S8→E8 (log2 TPM)
spt6S8→A8 (log2 TPM)
spt6-1004 (log2 TPM)
WT (log2 TPM)
B
WT vs spt6S8→E8
WT vs spt6S8→A8
WT vs spt6-1004
880
33
17
0
2
1
1
C
829 Genes
40 Genes
Distance from TSS (kb)
log2(Antisense Signal)
D
p < 0.0001
Average Normalized Antisense RNA−seq Signal (log2)
5' half of gene
3' half of gene
E
Genes with high 5' signal: 32
Genes with high 3' signal: 8
Number of Genes
Avg. 5' Antisense Signal/Avg. 3' Antisense Signal (log2)
F
p < 0.0001
Average, Normalized Antisense RNA−seq Signal (log2)
5' half of gene
3' half of gene
G
Genes with high 5' signal: 668
Genes with high 3' signal: 161
Number of Genes
Avg. 5' Antisense Signal/Avg. 3' Antisense Signal (log2)
H
1,000 bp
sense signal
antisense signal
WT
spt6S8→E8
spt6S8→A8
spt6-1004
VMA5
SMY1
DHR2
I
1,000 bp
sense signal
antisense signal
WT
spt6S8→E8
spt6S8→A8
spt6-1004
YTA6

Figure 3

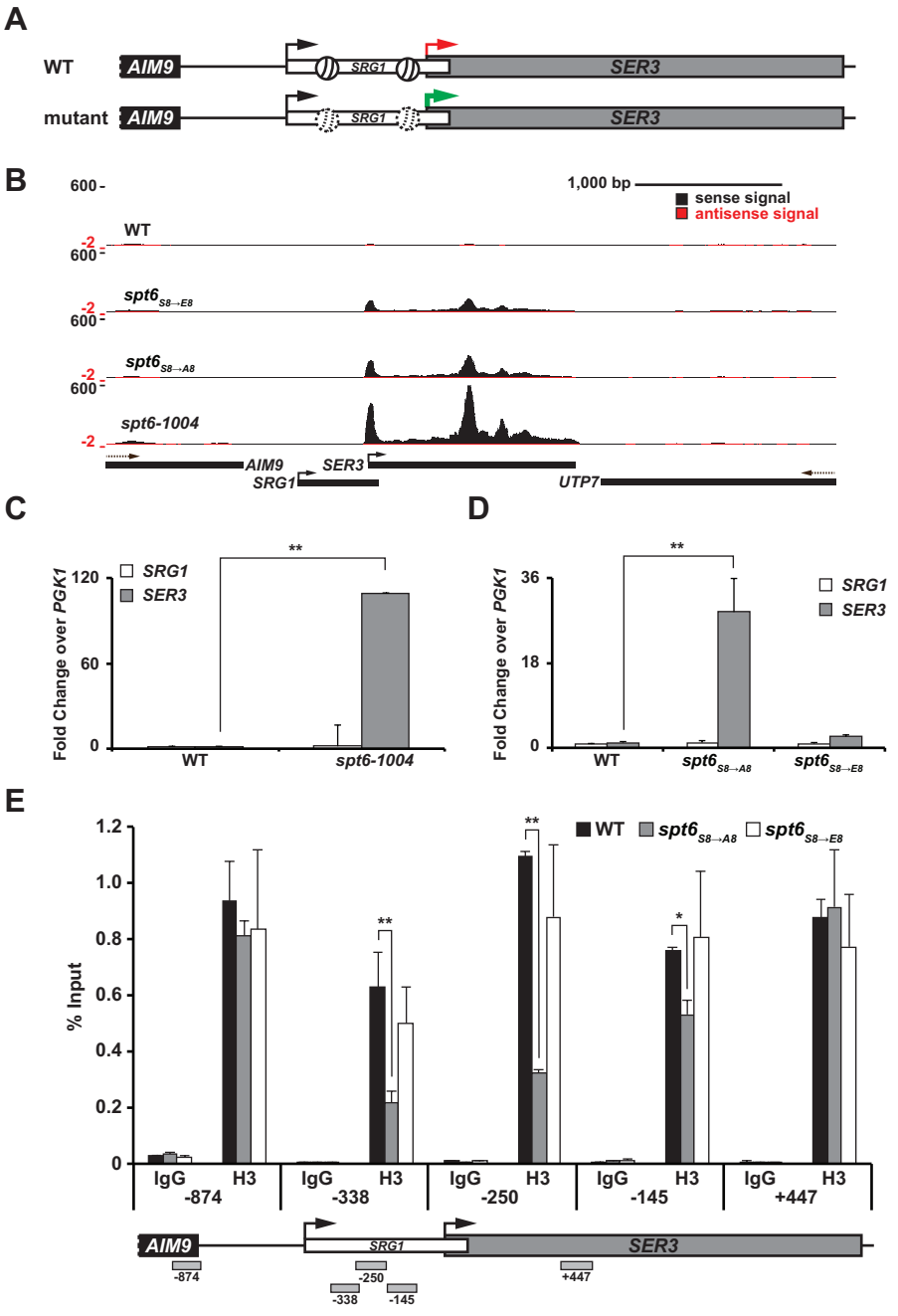
A
WT
AIM9
SRG1
SER3
mutant
AIM9
SRG1
SER3
B
600
1,000 bp
sense signal
antisense signal
WT
-2
600
spt6S8→E8
-2
600
spt6S8→A8
-2
600
spt6-1004
-2
AIM9
SRG1
SER3
UTP7
C
Fold Change over PGK1
120
60
0
SRG1
SER3
**
WT
spt6-1004
D
Fold Change over PGK1
36
18
0
SRG1
SER3
**
WT
spt6S8→A8
spt6S8→E8
E
% Input
1.2
1.0
0.8
0.6
0.4
0.2
0
WT
spt6S8→A8
spt6S8→E8
**
**
*
IgG
H3
-874
-338
-250
-145
+447
AIM9
SRG1
SER3
-874
-250
-338
-145
+447

Figure 4

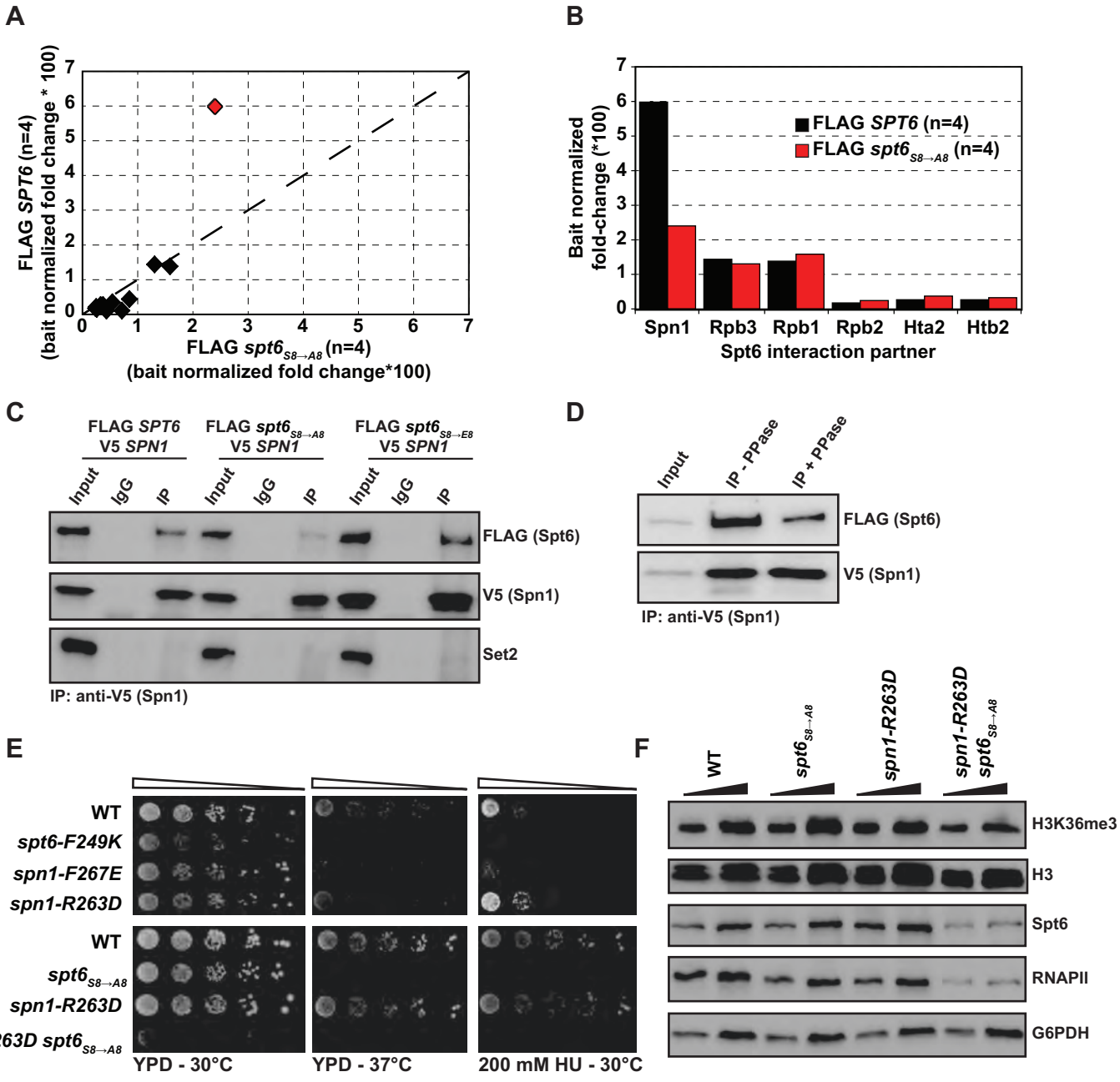
A
FLAG SPT6 (n=4)
(bait normalized fold change * 100)
FLAG spt6S8→A8 (n=4)
(bait normalized fold change*100)
B
Bait normalized
fold-change (*100)
FLAG SPT6 (n=4)
FLAG spt6S8→A8 (n=4)
Spn1
Rpb3
Rpb1
Rpb2
Hta2
Htb2
Spt6 interaction partner
C
FLAG SPT6
V5 SPN1
FLAG spt6S8→A8
V5 SPN1
FLAG spt6S8→E8
V5 SPN1
Input
IgG
IP
FLAG (Spt6)
V5 (Spn1)
Set2
IP: anti-V5 (Spn1)
D
Input
IP - PPase
IP + PPase
FLAG (Spt6)
V5 (Spn1)
IP: anti-V5 (Spn1)
E
WT
spt6-F249K
spn1-F267E
spn1-R263D
WT
spt6S8→A8
spn1-R263D
spn1-R263D spt6S8→A8
YPD - 30°C
YPD - 37°C
200 mM HU - 30°C
F
WT
spt6S8→A8
spn1-R263D
spn1-R263D spt6S8→A8
H3K36me3
H3
Spt6
RNAPII
G6PDH

Figure 5

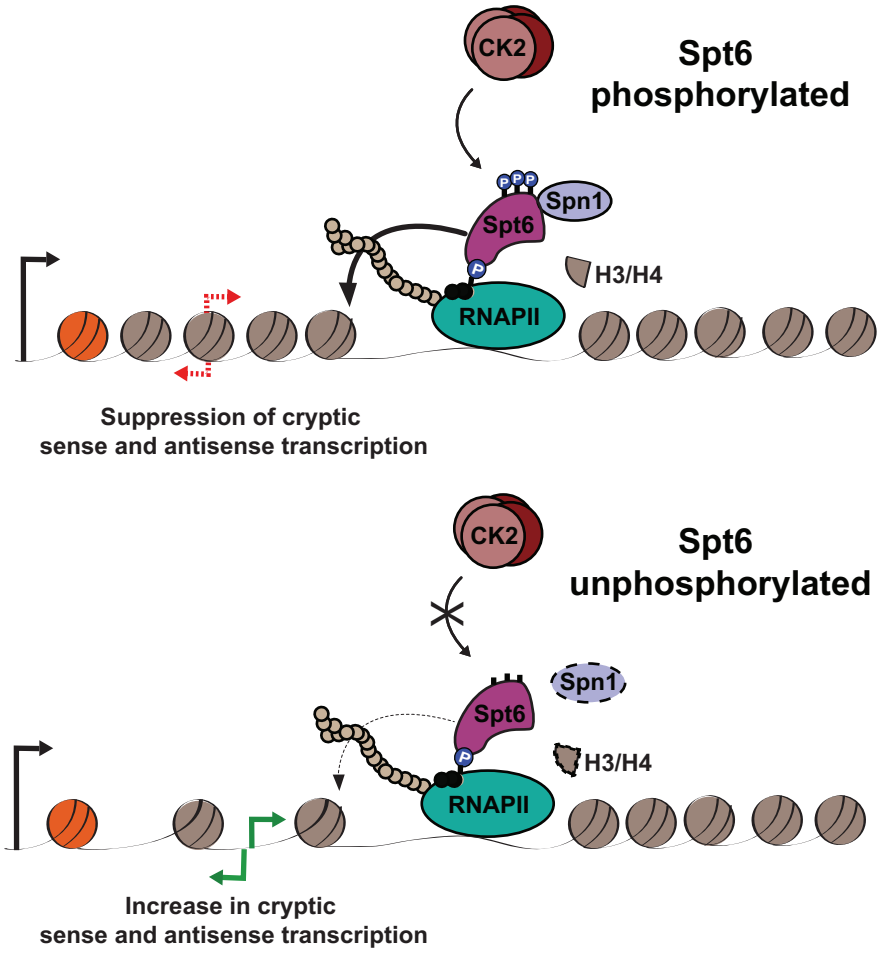
CK2
Spt6
phosphorylated
Spn1
Spt6
H3/H4
RNAPII
Suppression of cryptic
sense and antisense transcription
CK2
Spt6
unphosphorylated
Spn1
Spt6
H3/H4
RNAPII
Increase in cryptic
sense and antisense transcription

Figure 6

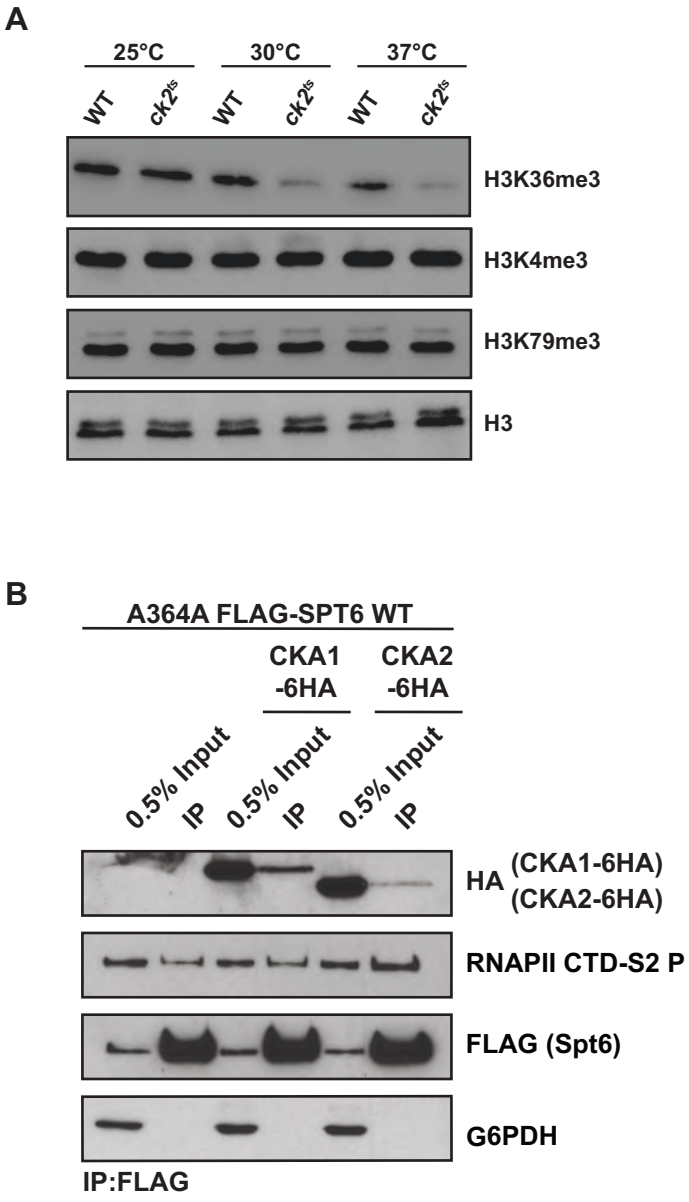

Supplementary Figure 1

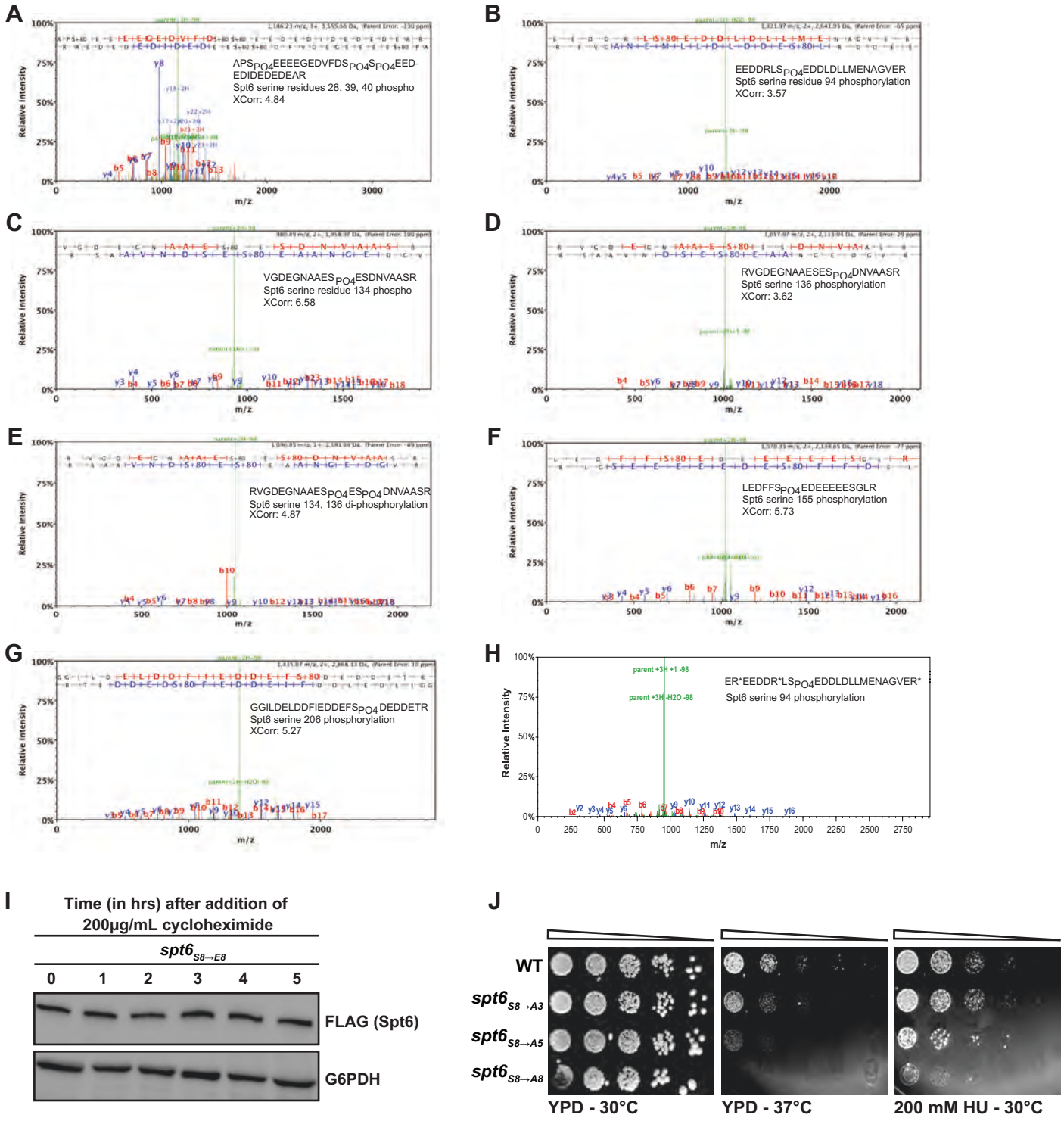

Supplementary Figure 2

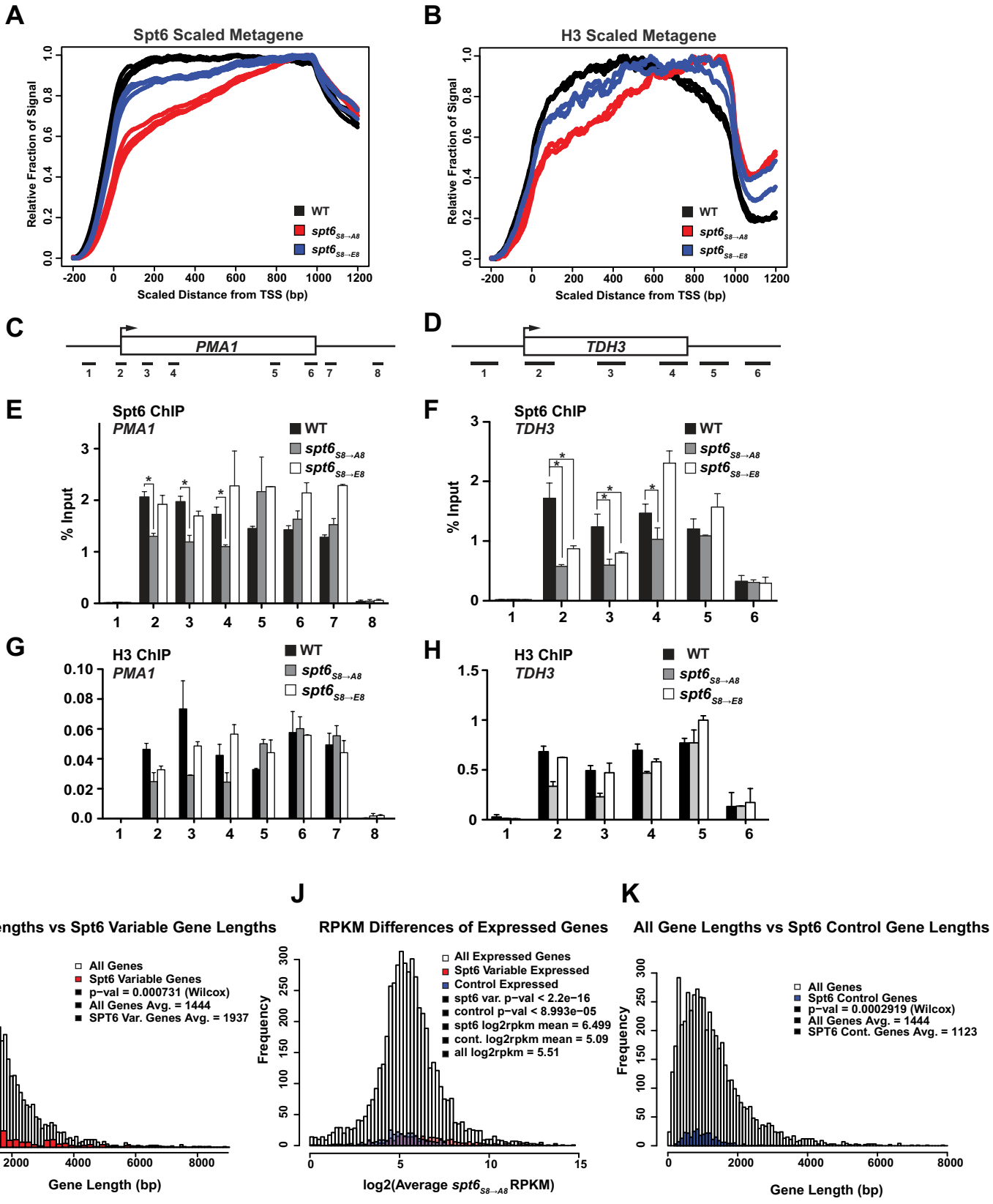

Supplementary Figure 3

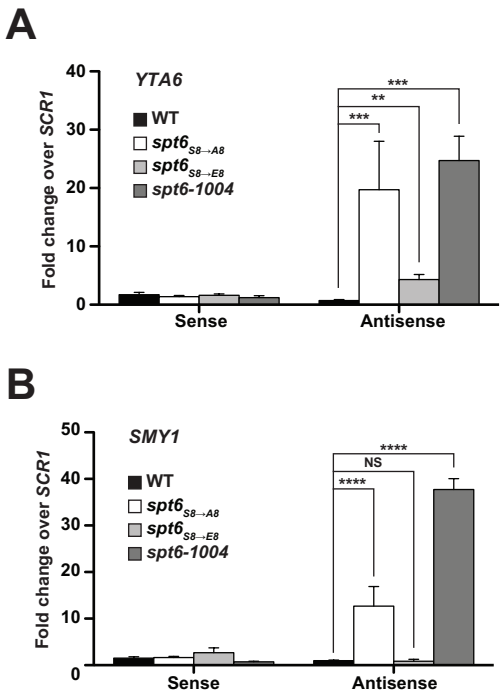

Supplementary Figure 4

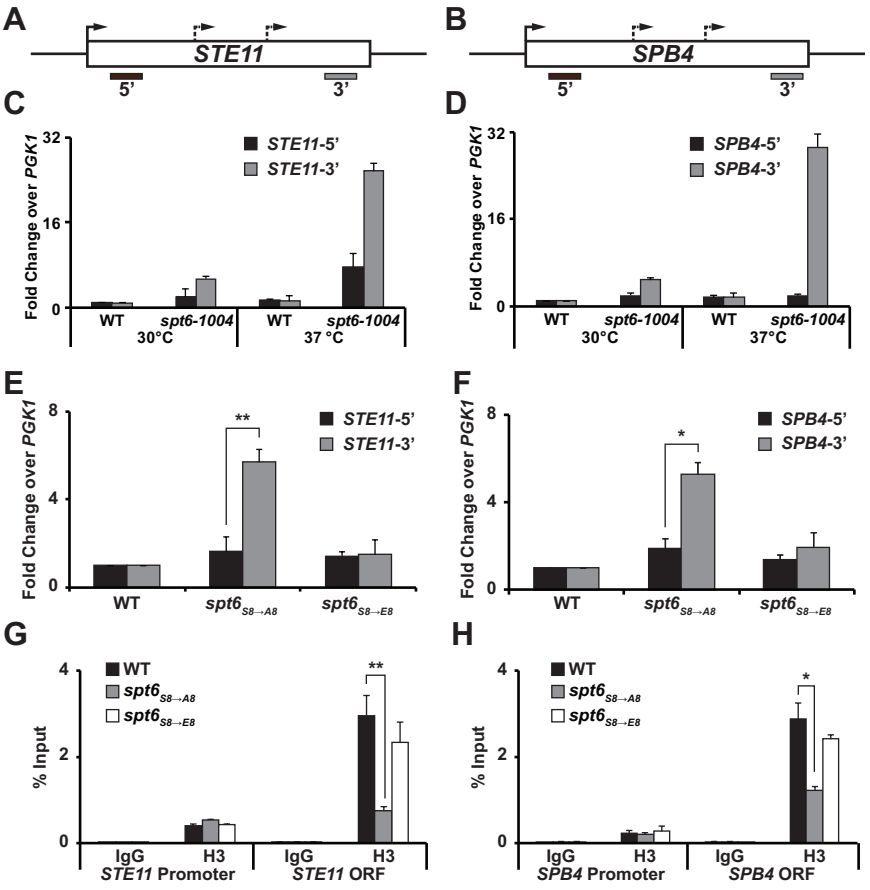

Supplementary Figure 5

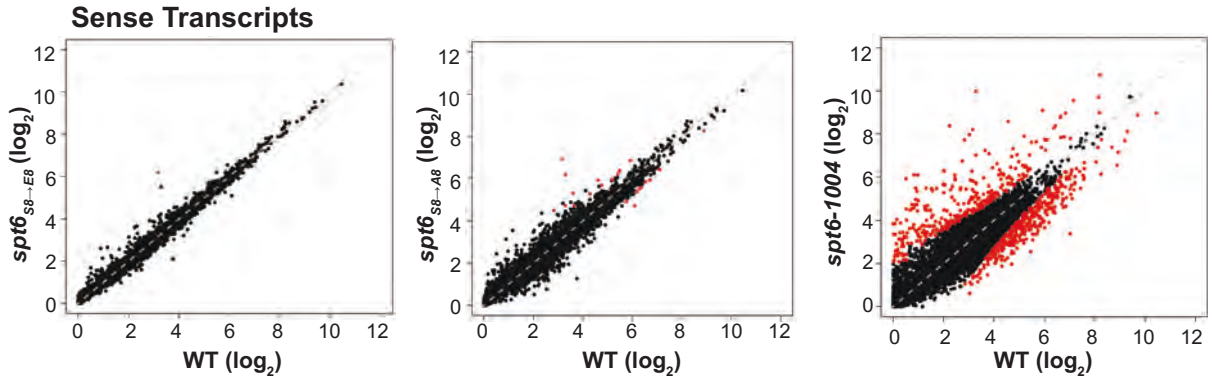

Supplementary Figure 6

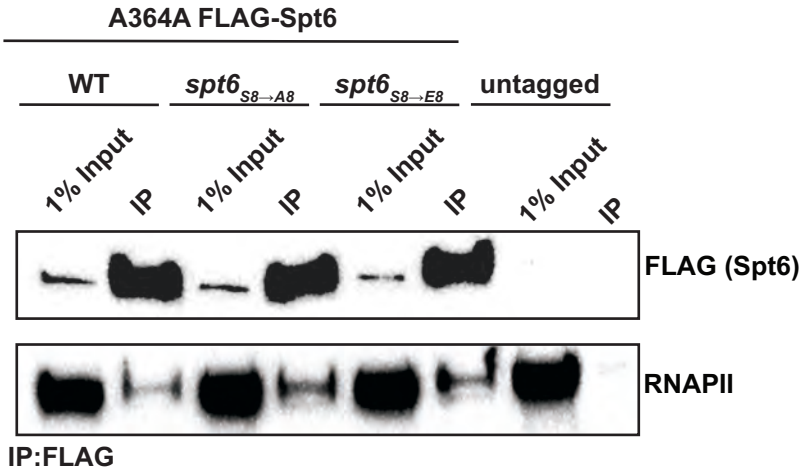

Supplementary Figure 7

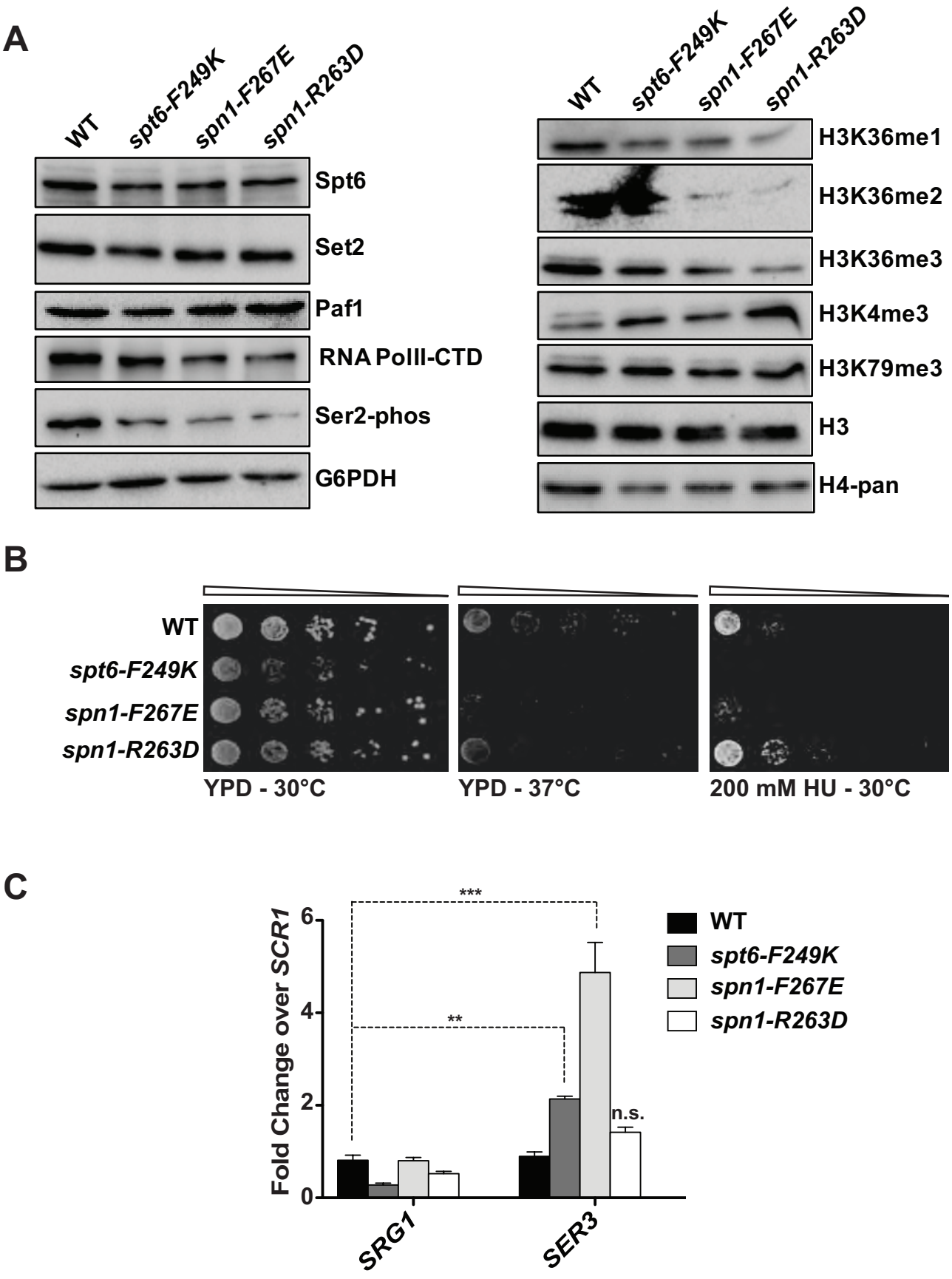

Supplementary Figure 8